

2016-12-27

# Bromine soil/sediment enrichment in tidal salt marshes as a potential indicator of climate changes driven by solar activity: New insights from W coast Portuguese estuaries

Moreno, J

<http://hdl.handle.net/10026.1/8425>

---

10.1016/j.scitotenv.2016.11.130

Science of The Total Environment

Elsevier BV

---

*All content in PEARL is protected by copyright law. Author manuscripts are made available in accordance with publisher policies. Please cite only the published version using the details provided on the item record or document. In the absence of an open licence (e.g. Creative Commons), permissions for further reuse of content should be sought from the publisher or author.*

1 **Bromine soil/sediment enrichment in tidal salt marshes as a potential indicator of**  
2 **climate changes driven by solar activity: new insights from W coast Portuguese**  
3 **estuaries**

4  
5 J. Moreno<sup>a,b,1</sup>, F. Fatela<sup>a,b</sup>, E. Leorri<sup>c</sup>, F. Moreno<sup>d</sup>, M.C. Freitas<sup>a,b</sup>, T. Valente<sup>e</sup>, M.F. Araújo<sup>f</sup>,  
6 J.J. Gómez-Navarro<sup>g</sup>, L. Guise<sup>e</sup> and W.H. Blake<sup>h</sup>

7  
8 <sup>a</sup> IDL - Instituto Dom Luiz, Universidade de Lisboa, Campo Grande, 1749-016 Lisboa,  
9 Portugal.

10 <sup>b</sup> Departamento de Geologia da Faculdade de Ciências da Universidade de Lisboa, Campo  
11 Grande, 1749-016 Lisboa, Portugal.

12 <sup>c</sup> East Carolina University, Department of Geological Sciences, Greenville, NC 27858-  
13 4353, USA.

14 <sup>d</sup> Independent researcher, Caminho da Portela, 97, 4940-061 Bico PCR, Portugal.

15 <sup>e</sup> Universidade do Minho, Centro de Investigação Geológica, Ordenamento e Valorização  
16 de Recursos, Departamento de Ciências da Terra, CIG-R, 4710-057 Braga, Portugal.

17 <sup>f</sup> Universidade de Lisboa, Instituto Superior Técnico, Centro de Ciências e Tecnologias  
18 Nucleares (C<sup>2</sup>TN), Estrada Nacional 10, km 139,7, 2695-066 Bobadela LRS, Portugal.

19 <sup>g</sup> Department of Physics, University of Murcia, Spain.

20 <sup>h</sup> School of Geography, Earth and Environmental Sciences, Plymouth University, Plymouth,  
21 Devon, PL4 8AA, UK

---

<sup>1</sup> jcmoreno@fc.ul.pt

22

23 **Abstract**

24 This paper aims at providing insight about bromine (Br) cycle in four Portuguese estuaries:  
25 Minho, Lima (in the NW coast) and Sado, Mira (in the SW coast). The focus is on their tidal  
26 marsh environments, quite distinct with regard to key biophysicochemical attributes.  
27 Regardless of the primary bromide ( $\text{Br}^-$ ) common natural source, i.e. seawater, the NW  
28 marshes present relatively higher surface soil/sediment Br concentrations than the ones  
29 from SW coast. This happens in close relation with organic matter (OM) content, and is  
30 controlled by their main climatic context. Yet, the anthropogenic impact on Br concentrations  
31 cannot be discarded. Regarding [Br] spatial patterns across the marshes, the results show a  
32 general increase from tidal flat towards high marsh. Maxima [Br] occur in the upper driftline  
33 zone, at transition from highest low marsh to high marsh, recognized as a privileged setting  
34 for OM accumulation. Based on the discovery of OM ubiquitous bromination in marine and  
35 transitional environments, it is assumed that this Br occurs mainly as organobromine.  
36 Analysis of two dated sediment cores indicates that, despite having the same age (AD  
37 1300), the Caminha salt marsh (Minho estuary) evidences higher Br enrichment than the  
38 Casa Branca salt marsh (Mira estuary). This is related to a greater Br storage ability, which  
39 is linked to OM build-up and rate dynamics under different climate scenarios. Both cores  
40 evidence a fairly similar temporal Br enrichment pattern, and may be interpreted in light of  
41 the sun–climate coupling. Thereby, most of the well-known Grand Solar Minima during the  
42 Little Ice Age appear to have left an imprint on these marshes, supported by higher [Br] in  
43 soils/sediments. Besides climate changes driven by solar activity and impacting marsh Br  
44 biogeodynamics, those [Br] positive peaks might also reflect inputs of enhanced volcanic  
45 activity covarying with Grand Solar Minima.

46

47 **Keywords:** Salt marshes; Br cycle; OM storage; Grand Solar Minima; Climate modelling;  
48 Climate variability.

49

## 50 **1. Introduction**

51 Wetlands play an important role on the biogeochemical cycle of elements such as carbon,  
52 nitrogen, phosphorus, sulphur and mercury at local, regional and even global scales (e.g.,  
53 Marques et al., 2011; Neubauer et al., 2013). A considerable amount of research has  
54 revealed that this is also true for bromine (Br) (Varner et al., 1999; Keppler et al., 2000;  
55 Rhew et al., 2000, 2002, 2014; Dimmer et al., 2000; Drewer et al., 2006; Manley et al.,  
56 2006; Hardacre et al., 2009, 2013; Blei et al., 2010; Martínez-Cortizas et al., 2007, 2016).  
57 Specifically, coastal wetlands, in which tidal marshes are included, represent important  
58 land-ocean-atmosphere interfaces that allow to capture spatiotemporal variability in  
59 chemical fluxes. In these habitats, Br mainly supplied by seawater interacts with both  
60 halophytes and the relatively large pool of soil/sediment organic matter (OM). This  
61 connection occurs through, although still poorly understood, bromination processes that  
62 contribute to the production of organobromine compounds, which have detrimental effects  
63 on the atmosphere. For instance, salt marshes have been identified as globally significant  
64 natural sources of methyl bromide (CH<sub>3</sub>Br) (Rhew et al., 2014, and references therein), a  
65 reactive trace gas contributing to ozone loss processes in the stratosphere (e.g.,  
66 Chipperfield, 2015). On the other hand, significant widespread bromination of natural OM  
67 may significantly impact the preservation and/or degradation of organic carbon (C<sub>org</sub>) in  
68 soils/sediments (Leri and Myneni, 2012), therefore affecting the recognized salt marsh  
69 ecosystem's role on climate and carbon sequestration. It is also known that in coastal (and  
70 open ocean) areas, bromine-radical chemistry provides alternative reaction pathways in the  
71 marine atmospheric boundary layer for (i) sulphur cycling, with associated implications for

72 aerosol production (and growth), radiative heat transfer and climate (Keene et al., 2007),  
73 and (ii) mercury (Hg) cycling (Obrist et al., 2011; Tas et al., 2012), with Br-induced mercury  
74 oxidation as a likely important Hg source to world's oceans, which can contribute to human  
75 mercury exposure by seafood consumption (Sunderland, 2007). Taking together the  
76 previous findings about the Br influence on other key element biogeochemical cycles in the  
77 marine domain, and the knowledge that natural CH<sub>3</sub>Br emissions are contributing to  
78 increase the stratospheric reactive Br budget (e.g., Carpenter et al., 2014), establishing the  
79 foundations of the Br biogeochemical cycle in coastal areas and tidal marsh habitats has  
80 gained a renewed significance.

81 Traditionally, Br has been used in conjunction with chlorine (Cl) as a geochemical proxy for  
82 seawater intrusion in coastal areas (e.g., Jones et al., 1999; Alcalá and Custodio, 2008),  
83 and alone as a paleosalinity indicator and a stratigraphic marker in brine cores (Adams,  
84 1969; Ziegler et al., 2008). An alternative interpretation regarding Br concentrations and  
85 fluxes has been proposed by Moreno et al. (2015) when studying the sedimentary record  
86 recovered from the high marsh zone on a tidal salt marsh located in the NW coast of  
87 Portugal (Caminha, in the Minho River estuary). They suggested that the most prominent Br  
88 enrichment peaks between AD 1300 (tidal marsh settlement) and AD 1800 (considered as  
89 the beginning of industrialization) were primarily driven by a series of biogeochemical  
90 processes rather than an indication of seawater intrusion events in the Minho estuary.  
91 Those processes responded to significantly prolonged environmental (e.g., temperature and  
92 precipitation) shifts triggered by Grand Minima Episodes of solar activity (SA) during the  
93 LIA, namely the Wolf and the Maunder Minima, as well as the Dalton Minimum. These  
94 episodes corresponded to periods of solar minimal energy output, as demonstrated by long-  
95 term records of SA proxies (e.g. Usoskin et al., 2007), affecting Earth's climate. Prolonged  
96 changes in environmental conditions can lead to significant responses at all levels of  
97 ecosystem organization, generating persistent alterations in its biogeochemical functioning

98 (e.g., Keller et al., 2006; Neubauer et al., 2013). Accordingly, and based on Moreno et al.  
99 (2015) that linked Br biogeodynamics to past SA, the impact of the sun–climate coupling at  
100 Grand Solar Minima resulted in cascading effects on Br cycling in the Caminha salt marsh,  
101 in parallel with rate changes in OM bromination, which ultimately weakened the marsh’s role  
102 as a source for CH<sub>3</sub>Br.

103 Following the study conducted in Caminha, the current contribution expands and  
104 generalises the analysis, including three other Portuguese estuaries (Figure 1): the Lima  
105 estuary, also in the NW coast, and the Sado and Mira estuaries, both located in the SW  
106 coast. Broadly, the Portuguese W coast is typically characterized by an Atlantic climate,  
107 though two main climatic regions can be distinguished. Compared to the NW coast, climate  
108 in SW coast has drier summers, lower annual precipitation as well as higher annual  
109 temperatures and insolation. Therefore, the aim of this work is twofold: (i) acquire a wider  
110 latitudinal range of Br measurements in waters (superficial and interstitial) and marsh  
111 soils/sediments in order to infer trends associated to the bio-geomorphological settings and  
112 climatic variability, and (ii) improve the understanding of bromine-climate relationships  
113 driven by SA, also providing new independent data and source insight to the still ongoing  
114 debate about the “missing source” for the CH<sub>3</sub>Br global budget (Yvon-Lewis et al., 2009).

115

## 116 **2. Regional setting**

### 117 ***NW coast***

118 Taken together, the Minho and Lima watersheds cover an area of 19 550 km<sup>2</sup> under an  
119 Atlantic wet climate, with relatively high exposition to maritime winds, high mean annual  
120 precipitations (Minho: 1200–2400 mm; Lima: 1300–4200 mm), mild summers (summer

121 mean temperatures from ca. 18–22°C) and relatively low mean annual insolation (2200–  
122 2500 hours) (APA, 2011).

123 The Minho estuary (23 km<sup>2</sup>) is oriented NE–SW and presents a semidiurnal, high-mesotidal  
124 regime in which vertical stratification occurs during periods of large freshwater discharge.  
125 The mean annual freshwater inflow is around 300 m<sup>3</sup>/s (Ferreira et al., 2003). The highest  
126 high water spring (HHWS) is 4 m height, but this is often amplified by storm surges  
127 (Taborda and Dias, 1991), which we observed during field work. The mean tidal range is of  
128 about 2.0 m. The upstream limit of the tidal salt wedge in the Minho River is 9 km (Fatela et  
129 al., 2009). Large tidal flat and tidal marsh surfaces with approximately 6 km<sup>2</sup> occur in the  
130 Minho estuary's banks, with its largest expansion along the left bank – Caminha tidal marsh  
131 (ca. 2.5 km<sup>2</sup>) – at the confluence with Coura tributary (Figure 1). Recently, Reis et al. (2014)  
132 updated the estuary ecological quality to “moderately to remarkably polluted” based on  
133 metal concentrations guidelines (SFT TA-1467/1997). Furthermore, the use of ethylene  
134 dibromide in leaded gasoline and the vehicle emissions since 1930, a shared Br and Pb  
135 anthropogenic source, appears to have had a significant impact on the Caminha salt marsh  
136 (Moreno et al., 2015).

137 The Lima estuary (5 km<sup>2</sup>), located 20 km south of Minho, is oriented ENE–WSW and it is a  
138 semidiurnal mesotidal estuary, with a mean tidal range of about 2.5 m and a HHWS of 3.7  
139 m (Vale and Dias, 2011). The mean annual freshwater inflow is 50 m<sup>3</sup>/s (Vale and Dias,  
140 2011). Here the tidal salt wedge effect is noticed to 3–5 km upstream in winter and no more  
141 than 15 km in summer (Alves, 2003). Intertidal areas extend over more than 2 km<sup>2</sup> on the  
142 banks of the Lima estuary, including the Nossa Senhora do Rosário salt marsh (NSR;  
143 Figure 1). The Lima lower estuary's ecological status is considered moderate (Costa-Dias et  
144 al., 2010). This results from the significant impact on the estuary of the harbour activities,  
145 leading to continuous petrochemical contamination (Lima et al., 2007), and diffuse pollution

146 from agriculture, domestic, and industrial waste discharges, including a paper mill (Costa-  
147 Dias et al., 2010).

148 The salt marshes of these two NW sites are classified as Eurosiberian, based on their plant  
149 communities (Costa et al., 2009), with abundant reed meadows where the presence of  
150 *Juncus maritimus* Lam. (C3 plant; non-succulent; perennial) is ubiquitous (Honrado et al.,  
151 2004; Almeida et al., 2011). Although, other plant species can also be found such as the  
152 non-native *Triglochin striatum* Ruiz & Pav. (C3 plant; succulent; perennial), the invasive  
153 *Phragmites australis* (Cav.) Trin ex. Steud. (C3 plant) and the weed *Spartina patens* (Aiton)  
154 Muhl (C4 plant; non-succulent; perennial) (Almeida et al., 2011).

155

## 156 **SW coast**

157 The SW coast of Portugal, where the Sado and Mira estuaries are located, is under a sub-  
158 wet Mediterranean climate, with mean values of annual precipitation around 600–700 mm  
159 (Bettencourt et al., 2003). Mean air surface temperatures are near 23°C in the hottest  
160 months (July and August), with a yearly average number of sunshine hours ranging 2900–  
161 3000 (APA, 2011), also showing almost permanent maritime moist winds (APA, 2011). The  
162 size of Sado and Mira rivers watersheds is 6 700 km<sup>2</sup> and 1 576 km<sup>2</sup>, respectively.

163 The Sado estuary (170 km<sup>2</sup>), the second largest estuarine system in Portugal, is located  
164 about 40 km south of Lisbon (Figure 1). It is a well-mixed estuary under normal river flow  
165 conditions, however, high discharge in some winter months may cause moderate  
166 stratification locally (Ferreira et al., 2003). It has a complex morphology generally oriented  
167 NW–SE and presents wide tidal flats as well as narrow and discontinuous coastal salt  
168 marshes covering around 7.2 km<sup>2</sup> (Moreira, 1992). The tidal pattern is semi-diurnal, with a  
169 mean tidal range of about 2.7 m and a HHWS of 3.2 m (Martins et al., 2001). The maximum



170 salt-wedge limit is 70 km upstream. The mean annual freshwater input is ca. 40 m<sup>3</sup>/s,  
171 exhibiting large interannual fluctuations. The lower estuary behaves as a coastal lagoon,  
172 while the upper reaches present a greater fluvial influence (Martins et al., 2001). In general,  
173 the Sado estuary can be classified as moderately contaminated, but the lower estuary and  
174 some segments near industrial areas have revealed levels of concern for several  
175 contaminants both organic and inorganic, with adverse toxicological effects to biota (e.g.,  
176 Neuparth et al., 2005).

177 Finally, the vertically well-mixed Mira estuary (4.5 km<sup>2</sup>) is a narrow incised estuary oriented  
178 NE–SW (e.g., Paula et al., 2006). It presents a semi-diurnal mesotidal regime with a mean  
179 tidal range of about 2.4 m and a HHWS of 3.5 m (Amaral et al., 2007). The salt edge may  
180 reach 32 km from the river mouth (Bettencourt et al., 2003). The lower section of the estuary  
181 has a dominant marine influence due to low, seasonal and limited freshwater input by the  
182 Mira River (2.9 m<sup>3</sup>/s). This characteristic has allowed the development in the lower 8 km of  
183 large, intertidal, and homogenous seagrass meadows of *Zostera noltii* Hornemann, 1832  
184 (e.g., Cunha et al., 2013). The estuarine area is also characterized by bare sandy areas and  
185 muddy substrates, with a 2.9 km<sup>2</sup> area of fringing salt marshes occurring as far as 15–20  
186 km upstream (Costa et al., 2001). These salt marshes have remained nearly unchanged  
187 since 1958, with the entire ecosystem relatively undisturbed by anthropogenic activities  
188 (Castro and Freitas, 2006).

189 As oppose to the NW sites, the SW salt marshes studied here belong to the Biogeographic  
190 Mediterranean region (Costa et al., 2009). The halophytic community is mixed including  
191 perennial succulent species such as *Halimione portulacoides* (L.) Aellen (C3 plant),  
192 *Sarcocornia fruticosa* (L.) A.J. Scott (C3 plant), *Sarcocornia perennis* (Mill.) A.J. Scott (C3  
193 plant) in the high marsh and the annuals *Spartina maritima* (Curtis) Fernald (C4 plant) and  
194 *Salicornia fragilis* P. W. Ball & Tutin (C3 plant) in the low marsh (e.g., Costa, 2001).

195

## 196 **2. Materials and Methods**

### 197 **2.1. Water and sediment samples**

198 The methodologies used for sampling and analysis of water (superficial and interstitial) and  
199 sediments (surface and cored) in the Lima, Sado and Mira estuaries follow Moreno et al.  
200 (2015) and are fully described therein. Figure 1 and Tables 1 and 2 summarize the new  
201 samples analysed here: eight interstitial water samples from three salt marsh transects  
202 (NSR\_L, TRO\_S, PMF\_M), ninety-one sediment surface samples from the intertidal domain  
203 (tidal flat, devoid of vascular plants; low marsh and high marsh zones with typical halophytic  
204 vegetation), along ten cross-shore transects, as well as an one-metre-long sediment core  
205 (hereafter FWCB<sub>r</sub>) recovered with a manual Auger sampler from the Casa Branca salt  
206 marsh (1.74 m above mean sea level; 37°40'03.7" N and 8°43'12.7" W), located on the Mira  
207 River estuary. A total of thirty sliced (1 cm thick) samples were analysed for Br and OM  
208 contents. The FCPw1 core from Moreno et al. (2015), located in the Caminha high marsh  
209 zone (1.55 m above mean sea level; 41°52'37.0" N and 8°49'28.0" W), is also indicated in  
210 Figure 1.

211 In order to characterize the two possible end-members (fluvial and marine) of  
212 biogeochemical sources to salt marshes, four marine seawater and four fluvial freshwater  
213 samples were collected (Table 1).

214 Water sample analyses: The filtrate was analysed for bromide (Br<sup>-</sup>), amongst other anions,  
215 by ion chromatography (IC) with suppressed conductivity detection (761 Compact IC  
216 Metrohm), and raw data processed with Metrohm Metro data 1.1. The IC method no. S-73,  
217 developed by Metrohm to determine anions in seawater, was used for the most saline  
218 waters (see Valente et al., 2009 and Moreno et al., 2015 for detailed information). A set of

219 standards was prepared to make a 6-point calibration curve covering the range of Br<sup>-</sup> (and  
220 Cl<sup>-</sup>) concentrations in water samples. The IC method not only allows an efficient separation  
221 of the Br<sup>-</sup> and Cl<sup>-</sup> peaks, but has also the advantage of measuring both anions in the same  
222 sample preventing the errors introduced by dilution. A standard (20 mg/L) was run  
223 independently of the calibration curve to check for accuracy (every two samples) and  
224 sample replicates were run to check for precision. The precision was within the relative  
225 standard deviation (RSD) of 5% for all determinations and results were accurate within  
226 precision.

227 Sediment sample analysis: Br concentrations in cored samples, along with the collected  
228 surface sediments, were determined by Energy-Dispersive X-Ray Fluorescence  
229 Spectrometry (EDXRF), using a KEVEX 771 spectrometer. To calibrate the spectrometer  
230 and verify the accuracy and precision of the overall procedure three certified reference  
231 materials were analysed: SGR1 (Green River Shale from the United States Geological  
232 Survey – USGS), SRM 2704 (Buffalo River Sediment) and SRM1646 (Estuarine Sediment),  
233 both from the National Institute for Standards and Technology (NIST). A complete  
234 description of the equipment, analytical conditions and spectral evaluation, along with the  
235 calibration and quantification techniques, is available in Araújo et al. (1998, 2003). Accuracy  
236 and precision on the Br determinations are better than 10% as previously fully described in  
237 Moreno et al. (2015). The OM content was determined as Loss-on-Ignition (LOI), with an  
238 aliquot of bulk sediment sample (2.0 g) dried and oven-heated at a temperature of 500 °C ±  
239 50 °C for about 2 hours (Moreira et al., 2009). Quality control was checked by replicate  
240 analysis (40% of the total), with errors lying in the interval 0.1%–15.0% (average: 5.7%) of  
241 the measured value. In an attempt to test the reliability of LOI data for the estimation of C<sub>org</sub>  
242 content, a regression analysis was performed for LOI vs. C<sub>org</sub> for the FCPw1 core, with C<sub>org</sub>  
243 data taken from de la Rosa et al. (2012). A strong statistically significant correlation ( $r= 0.97$ ,

244 N= 19;  $p < 0.001$ ) between LOI and  $C_{org}$  was achieved, ensuring that LOI results are  
245 reflecting mostly  $C_{org}$  (%OM).

246 In order to characterize OM quality, i.e. the percentages of labile and recalcitrant OM, the  
247 stepwise thermogravimetric procedure (STG) of Kristensen (1990) was applied to the cored  
248 samples from the Casa Branca salt marsh. According to this method, these OM fractions  
249 are defined as the percentage weight losses after ignition at 280°C and 520°C, respectively.  
250 In short, samples of 0.5 g were grounded and pre-dried at 105°C for 6h. After cooling in a  
251 desiccator, the sample weight was determined with a precision of 0.1 mg. Next, the samples  
252 were combusted at precisely 280°C for 6h in a computer controlled Heraeus MR 170 muffle  
253 furnace. After cooling in a desiccator and re-weighing, the samples returned to the muffle  
254 furnace and combusted at 520°C for 6h. After cooling in a desiccator the final ash weight  
255 was determined (Kristensen, 1990).

256

## 257 **2.2. Solar activity, temperature, and precipitation climatic modelled data**

258 Cosmogenic radionuclides are produced in the atmosphere through a nuclear cascade  
259 mainly triggered by the high-energy galactic cosmic rays (GCR; Lal and Peters, 1967). As  
260 GCR enter the heliosphere, they are subject to modulation processes due to variable solar  
261 magnetic activity. This is the reason why during phases of low SA much higher particle  
262 intensities occur inside the heliosphere than during solar maximum conditions (e.g., Herbst  
263 et al., 2015; Adolphi and Muscheler, 2016). The two most noticeable cosmogenic  
264 radionuclides suitable for reconstructing SA are  $^{14}\text{C}$  and  $^{10}\text{Be}$ . The production rate of both  
265 isotopes reacts in a very similar way to changes in solar and geomagnetic shielding  
266 (Masarik and Beer, 1999). The reconstructed dataset chosen for this work is the total solar  
267 irradiance (TSI), considered as a proxy for SA, from Steinhilber et al. (2012). This

268 reconstruction is based on time series of  $^{14}\text{C}$  stored in tree rings and of  $^{10}\text{Be}$  extracted from  
269 polar ice cores, and was downloaded from the NOAA web page (<http://www.noaa.gov/>).

270 Aiming to compare the Br and OM records with climate variables, this study also  
271 incorporates the series of temperature and precipitation evolution in both study areas as  
272 predicted by a high-resolution regional climate model (Gómez-Navarro et al., 2011). The  
273 simulation implements a domain that encompasses the whole Iberian Peninsula (IP) and  
274 spans the second millennium entirely. It was carried out with a climate version of the  
275 mesoscale model MM5, and driven at the boundaries by a simulation with the global model  
276 ECHO-G (see Gómez-Navarro et al., 2011 for details). Following Gómez-Navarro et al.  
277 (2011), the use of a high resolution model aims to reduce the scale gap between the large-  
278 scale correctly simulated by the GCM and the features of regional variability present in the  
279 Br and OM records presented here. The model simulates coherently the evolution of most  
280 relevant climate variables, and in particular reproduces the physically constrained co-  
281 evolution of temperature and precipitation, as well as their relation with large-scale  
282 dynamics (e.g., the North Atlantic Oscillation – NAO). It is jointly driven by reconstructions of  
283 the variability of three external forcings: TSI, greenhouse gas concentrations and the effect  
284 of volcanic activity.

285

### 286 **2.3. Chronology**

287 The geochronology of the top 15 cm of the FWCBBr core was calculated from the  $^{210}\text{Pb}$   
288 profile using the constant rate of supply method (CRS) (Appleby and Oldfield, 1978)  
289 supported by  $^{137}\text{Cs}$ . Samples for  $^{210}\text{Pb}$  and  $^{137}\text{Cs}$  were analyzed following the methodology  
290 described by Appleby (2001) at the University of Plymouth (UK) Consolidated Radioisotope  
291 Facility, using an EG&G Ortec planar (GEM-FX8530-S N-type) HPGe gamma spectrometry

292 system built to ultra-low background specification for  $^{210}\text{Pb}$  detection. Additional  
293 information regarding the technique is provided in Appendix A. This core presented an  
294 unsupported  $^{210}\text{Pb}$  ( $^{210}\text{Pb}_{\text{xs}}$ ) profile that suggested some changes in the sediment  
295 accumulation rate in the upper section (ca. 150 years), although they could also reflect  
296 sediment mixing or disruption of the sedimentation. While the available elemental data is  
297 limited and presents generally low concentrations, the Pb profile shows slightly higher  
298 values above 18 cm that could be coincident with the initial stages of the industrial  
299 revolution (unclear date for this region but ca. AD 1800), which would be in agreement with  
300 the CRS model used here. However, the inflexion indicated by the model for the two older  
301 samples should be considered carefully (Leorri et al., 2010). In order to extend the  
302 chronology down-core, two samples (69–70 cm, 90–91 cm depth) of total organic carbon  
303 (TOC) were carbon-14 dated by accelerator mass spectrometry–AMS at Beta Analytic Inc.  
304 (USA). The chronology for the FWCB core was created using a Bayesian age-depth model  
305 (Bchron 4.1; Haslett and Parnell, 2008; Parnell et al., 2008) (Appendix A). The model  
306 provides ages with an individual error for each sample averaging 73 years for a 95%  
307 confidence interval. The obtained calendar ages are presented in years of *Anno Domini*  
308 (years AD).

309 The chronology of the FCPw1 core can be found in Moreno et al. (2015), but also relies on  
310 the combination of  $^{210}\text{Pb}$  and carbon-14 data from TOC.

311

### 312 **3. Results and discussion**

#### 313 **3.1. $\text{Br}^-$ in surface and interstitial water samples**

314 The results of  $\text{Br}^-$  concentrations in surface and interstitial waters are presented in Table 1.  
315 Freshwater samples show  $\text{Br}^-$  contents between less than 0.01 mg/L (Minho River) and a

316 maximum of 0.8 mg/L (Sado River). On the other hand, marine surface water samples  
317 throughout the W coast have Br<sup>-</sup> contents ranging from 185 to 197 mg/L (Table 1). Such  
318 high values, outside the typical marine [Br<sup>-</sup>] range: 60–80 mg/L, are somewhat expected  
319 and connected or linked to the known supersaturation in brominated organic compounds in  
320 the Portuguese offshore (Raimund et al., 2011). This is related to the presence of strong  
321 macroalgal sources and to the Iberian Peninsula coastal upwelling, as discussed previously  
322 by Moreno et al. (2015). Brominated organic compounds (also including CH<sub>3</sub>Br) are  
323 produced and degraded at relatively fast rates in the coastal ocean, with their degradation  
324 mechanisms (e.g., hydrolysis and chloride exchange reactions) in the water column as  
325 major suppliers of bromide anions to seawater. Our hypothesis – linking the Br<sup>-</sup> enrichment  
326 of western Portuguese superficial coastal waters to loss reactions of brominated organic  
327 compounds in seawater column – may be supported by other authors' findings. Namely, Hu  
328 et al. (2010) discovered for the east coast of United States evidence of a vertical distribution  
329 in the CH<sub>3</sub>Br saturation anomalies, with highest concentrations in the subsurface seawater  
330 below the mixed layer, due to high degradation rates near the surface. An analogous  
331 subsurface seawater enhancement in depth profiles of two of the most important short-lived  
332 carriers of atmospheric Br, i.e. dibromomethane (CH<sub>2</sub>Br<sub>2</sub>) and bromoform (CHBr<sub>3</sub>), was  
333 described by Raimund et al. (2011) when sampling the Iberian Peninsula upwelling system  
334 off the coast of Portugal.

335 The detected Br<sup>-</sup> enrichment in the nearshore surface water samples also implies that  
336 marine water would have Cl<sup>-</sup>/Br<sup>-</sup> mass ratios lower than the reported value for the average  
337 seawater (typically 290 ± 4; e.g., Katz et al., 2011). This chemical signature in our water  
338 samples is presented in the plot of Cl<sup>-</sup>/Br<sup>-</sup> mass ratios versus Cl<sup>-</sup> in Figure 2, along with a  
339 typical marine water sample (TA\_SW: [Cl<sup>-</sup>] = 19,353 mg/L and [Br<sup>-</sup>] = 67 mg/L; Millero,  
340 2013). The clusters displayed by the Cl<sup>-</sup>/Br<sup>-</sup> vs. Cl<sup>-</sup> plot allow to identify freshwater (with  
341 consistently lower levels of Cl<sup>-</sup> and Br<sup>-</sup>) from marine and brackish waters reflecting an

342 increase in  $\text{Cl}^-$  (Figure 2A). In addition, it is possible to differentiate between the interstitial  
343 water samples of the NW coast salt marshes (Minho and Lima) and the SW coast samples  
344 (Sado and Mira) (Figure 2B). This suggests that beyond the inferred common main source  
345 of  $\text{Br}^-$  (and  $\text{Cl}^-$ ), i.e., seawater (theoretical ranges after Panno et al., 2006), a clear N–S  
346 differentiation can be established based on the relationship between the chemical indicators  
347 chloride and bromide. As shown in Figure 2B, the Sado and Mira interstitial waters, ranging  
348 from polyhaline (18–30‰) to euhaline (30–40‰), can be considered closer, based on these  
349 anions, to marine water samples (all clustering together; Figure 2B) than the ones from the  
350 Caminha and Lima salt marshes (mostly mesohaline: 5–18‰). These results are  
351 symptomatic of a stronger mixing with freshwater, originated by higher inputs of rainfall-land  
352 runoff production to the NW coast salt marshes, leading to salt dilution and lower ionic  
353 concentrations.

354 At this point, it must be emphasized that a rising body of evidence suggests that  $\text{Br}^-$  does  
355 not act conservatively in soils or water.  $\text{Br}^-$  can be (re)actively involved in OM cycling (e.g.,  
356 Gerritse and George, 1988; Mahn and Gieskes, 2001; Biester et al., 2004, 2006; Leri et al.,  
357 2010, 2014), and it is frequently related to Fe and Mn cycling (e.g., Leri et al. 2010). This  
358 could diminish the “sensitivity” of the ratio  $\text{Cl}^-/\text{Br}^-$ , and limits its applicability as an inorganic  
359 tracer of marine intrusion. However, plotting  $\text{Cl}^-/\text{Br}^-$  ratios provides insight into the  $\text{Br}^-$  (and  
360  $\text{Cl}^-$ ) major sources in the sampled salt marshes. Panno et al. (2006) proposed  $\text{Cl}^-/\text{Br}^-$   
361 fingerprinting as a valuable diagnostic method in the identification of anthropogenic sources  
362 of salinization; though additional analysis should be required to complement this technique,  
363 and thus determine more accurately the source of the contaminant present in water  
364 samples. For instance, Figure 2B depicts a group of samples that evidence an  
365 anthropogenic impact based on this methodology – NSR\_P1 (tidal flat; Lima), TRO\_P7  
366 (high marsh zone; Sado) and PMF\_P6 (high marsh zone; Mira). The three fit in the “basin  
367 brines and animal waste” water-type (Panno et al., 2006). In addition, the sample TRO\_P7



368 presents a measurable  $[\text{NO}_3^-]$  of 54 mg/L, by opposition to the other two, both with  $[\text{NO}_3^-] <$   
369 0.01 mg/L (results not shown). Historical Br anthropogenic sources such as emissions from  
370 an antiknock additive in leaded gasoline, flame retardants, dyes, pharmaceuticals or  
371 pesticides in agriculture are well-known (e.g., Flury and Papritz 1993), and while some were  
372 phased out, others are still in use (e.g., Shaw et al., 2010). As briefly pointed in Section 2,  
373 the Lima, Sado and Mira estuaries have their specific histories of anthropogenic  
374 disturbances, but the effort to better distinguish the likely detected  $\text{Br}^-$  contamination in  
375 water samples (Figure 2B) is beyond the scope of the present study.

376

### 377 **3.2. Br-OM relationships in marsh surface environments**

378 The data gathered in the newly investigated salt marshes regarding interstitial waters (Table  
379 1) are scarce due to several sampling and analytical constraints. This, together with the  
380 presence of samples disturbed by anthropogenic activities frustrated our goal of broadening  
381 the “evidence base” for natural  $[\text{Br}^-]$  interstitial water patterns in salt marshes. It was earlier  
382 detected in the Caminha salt marsh that a pattern appears to be mainly dictated by marine  
383 influence (periodic tidal flooding), i.e., higher  $[\text{Br}^-]$  in low marsh zone (average 71 mg/L;  
384 Table 1), exposed to longer inundation periods by seawater and, consequently, prone to  
385 greater inflow of bromide (Moreno et al., 2015). This is correlated with the relative  
386 submersion times (annual basis) in the Caminha salt marsh, which is ca. 76–53% for tidal  
387 flat, ca. 53–10% for low marsh and ca. 10–2% for the high marsh (Fatela et al., 2009).

388  $\text{Br}^-$  entering salt marshes can be cycled by several biotic and abiotic OM bromination  
389 mechanisms (e.g., Keppler et al., 2000, 2004; Hamilton, 2003; Saito and Yokouchi, 2006;  
390 Wishkerman et al., 2008; Leri et al., 2010; Leri and Myneni, 2012; Leri and Ravel, 2015). All  
391 include the production of an oxidized form of Br that reacts with electron-rich organic

392 molecules, with the subsequent formation of organobromine by-products (Leri et al., 2014).  
393 Among them, it is the highly volatile gas CH<sub>3</sub>Br (e.g., Wuosmaa and Hager, 1990; Hamilton  
394 et al., 2003; Keppler et al., 2000, 2004; Saito and Yokouchi, 2006). Therefore, both the  
395 halophytic vegetation cover and the soil/sediment organic fraction of tidal salt marshes are  
396 the main settings and substrates for the conversion of inorganic Br (Br<sub>inorg</sub>) into organic Br  
397 (Br<sub>org</sub>), which can largely contribute to their Br pool (Moreno et al., 2015). It also explains  
398 why the total [Br] in (coastal) soils/sediments might not necessarily correlate with [Br<sup>-</sup>] in  
399 water (Leri and Ravel, 2015). This lack of correlation is clear in the investigated salt  
400 marshes, where some mismatch is observed between [Br<sup>-</sup>] in interstitial waters and the total  
401 [Br] gradient in surface soils/sediments (Tables 1 and 2; Figure 3). The highest total Br  
402 concentrations were found in the high marsh zones from Minho (average: 389 mg/kg) and  
403 Mira (avg.: 233 mg/kg) estuaries, while in their respective low marshes these contents did  
404 not exceed, on average, 133 mg/kg and 152 mg/kg (Table 2). Salt marshes from the Sado  
405 are the most depleted in both Br and OM, with average (median) values of 53 mg/kg and  
406 8.2% (low marsh), and 81 mg/kg and 11.7% (high marsh), respectively. In the Lima estuary,  
407 Br trends are quite distinct (Table 2). This might be explained by the dominance of a coarser  
408 soil/sediment fraction (mainly sands) in the samples from these salt marshes transects  
409 (results not shown). Since a direct correlation has been well-established and widely  
410 accepted between mud (clay and/or silt) grain size fractions and both Br (e.g., Correns,  
411 1956; Vinogradov, 1959) and OM (e.g., Buchanan and Longbottom, 1970; Mayer, 1994)  
412 contents, Br concentrations can be diluted in coarse-grained samples. The NSR\_L transect  
413 is additionally impacted by a dredged sand processing facility located in the marsh  
414 surrounding area, causing resuspension of large quantities of sediment and disturbing this  
415 salt marsh (Cardoso et al., 2008).

416 The spatial pattern across soil/sediment surface transects (Figure 3) presents a strong  
417 direct correlation between Br and %OM (Lima:  $r = 0.89$ ;  $N = 28$ ;  $p < 0.001$ ; Minho:  $r = 0.86$ ;

418 N= 21;  $p < 0.001$ ; Mira:  $r = 0.79$ ; N= 29;  $p < 0.001$ , and Sado  $r = 0.67$ ; N= 34;  $p < 0.001$ ; tidal  
419 flat samples are also included in the computed correlation coefficients). These results are in  
420 good agreement with other studies (e.g., Cundy et al., 2005), suggesting that elevation is a  
421 key factor controlling the soil/sediment  $C_{org}$  pools of tidal salt marshes, as suggested by  
422 Spohn and Giani (2012, 2013). These authors not only have found higher  $C_{org}$  stocks in the  
423 high marsh zones with limited flooding, but a major contribution of autochthonous (in situ)  
424 OM inputs of the halophytic plant cover to soils and sediments at higher elevation within the  
425 tidal frame. Such findings could likewise enlighten the preferential total Br enrichment in the  
426 surface soils/sediments from the studied high marshes. Assuming that this Br is present  
427 mainly as organobromine, the higher concentrations found in the high marsh zones,  
428 typically characterized by greater density of stems and litter, can be associated to the  
429 relatively fast oxidation of part of  $Br^-$ , which seems to lead to a rapid conversion to  $Br_{org}$   
430 (Leri and Myneni, 2012).

431 Similarly, the role of vegetation should be highlighted. The ubiquity of non-succulent  
432 perennial species (*Juncus maritimus*) in the Caminha and Lima salt marshes contrasts with  
433 the dominance of succulent species (e.g., from *Sarcocornia/Salicornia* genera) in Sado and  
434 Mira salt marshes. Manley et al. (2006) and Blei et al. (2010) found higher relative Br  
435 contents in succulent species, which (succulence) results from their strategy to survive in  
436 saline soils by maintaining a large amount of tissue water. According to Manley et al.  
437 (2006), high Br tissue levels would make of these succulent halophytes prolific  $CH_3Br$   
438 producers, although suggesting that each plant species has very different intrinsic abilities  
439 to produce  $CH_3Br$ . Blei et al. (2010) showed that the variations in the Br content found on  
440 salt marsh vegetation do not explain the spatial differences in  $CH_3Br$  flux magnitudes,  
441 concluding instead that the limiting factor lies on the plants conversion mechanism (abiotic  
442 and/or biotic). Wishkerman et al. (2008) reported that the abiotic reaction (occurring  
443 between plant pectin and Br followed by  $CH_3Br$  emission) is strongly influenced by both air

444 temperatures, increasing by a factor of two for every 5°C increase, and plants succulence,  
445 becoming more efficient as plants dry out. Rhew et al. (2014) estimated that only  
446 approximately 0.17% Br in the leaf tissue of *Batis maritima* L. (known as one of the CH<sub>3</sub>Br  
447 greatest producers in salt marshes) is daily removed via CH<sub>3</sub>Br emissions, indicating that to  
448 impact Br availability, a small separated subset of “active Br” at the enzyme site would be  
449 needed. According to them, if this *active* Br pool was 0.5% of the overall tissue content, then  
450 CH<sub>3</sub>Br emissions could reduce daily that pool by 34% for Br. This ongoing discussion is of  
451 major importance as it holds the power for unbalancing the total [Br<sup>-</sup>] (either reducing or  
452 increased it) available to ultimately be converted in Br<sub>org</sub> in a given marsh. As a final remark  
453 we would like to draw attention to the extensive intertidal habitat of *Zostera noltii* in Sado  
454 and Mira estuaries (Cunha et al., 2013), and its possible impact on the Br estuarine cycling.  
455 This seagrass along with *Zostera marina* Linnaeus 1753, which though very rare occurs as  
456 well in the Mira estuary (Cunha et al., 2013), also have been identified as  
457 producers/emitters of volatile Br compounds, such as CH<sub>3</sub>Br and CHBr<sub>3</sub> (Weinberg et al.,  
458 2013, 2015).

459 Interestingly, maximum Br soil/sediment enrichment in all studied salt marshes occurs in the  
460 highest low marsh transitioning to high marsh, in the so-called upper driftline zone (Adam,  
461 1990; Gerlach 1999; Persicke et al. 1999; Lefeuvre et al., 2000; Gettner, 2003). These  
462 areas represent a tidal-terrestrial/freshwater transition interface, where most drift litter  
463 accumulates, usually containing a high concentration of seeds and vegetative material  
464 (Mineke and Bakker 2002). While this litter is effectively taken out of the estuarine  
465 circulation (e.g., Boorman, 2003), it becomes potentially accessible for promoting the  
466 magnification of the local C<sub>org</sub> pool of soils/sediments. As a result, and even if the  
467 understanding of the internal marsh processes affecting OM accumulation and turnover is  
468 limited (Fagherazzi et al., 2013) – identical to the mechanisms regulating Br<sup>-</sup> fluxes –, it  
469 seems plausible to consider the upper driftline zones as promising Br<sub>org</sub> sink areas, from the

470 standpoint of the current knowledge about OM bromination. Driftline zones might also be  
471 natural laboratories for studying the short and longer-term impacts of counterbalancing  
472 controls, like temperature, moisture and inundation (e.g., Lewis et al., 2014) as well as  
473 priming (e.g., Gontikaki et al., 2013) on OM mineralization, distressing Br sequestration and  
474 its fate in coastal environments.

475 Finally, the identified Br reduction in the soils/sediments collected at the highest high marsh  
476 (Figure 3) can be attributed to the increased influence of adjacent terrestrial uplands, taking  
477 into account the principle that the terrestrial environment, and thus terrestrial OM, is  
478 relatively poor in bromine (Mayer et al., 2007).

479

### 480 **3.2. Br temporal trends in SW (Mira estuary) and NW (Minho estuary) coasts**

#### 481 *3.2.1. Comparing Br enrichment in relation to the long-term OM storage ability from salt* 482 *marshes in their soils/sediments*

483 Casa Branca salt marsh (FWCBr core; Mira estuary) down-core profiles of Br and OM up to  
484 89 cm depth (AD 1190) are presented in Figure 4, along with the profiles previously  
485 obtained from the Caminha salt marsh up to 62 cm depth (AD 1143) (FCPw1 core; Fig. 3 of  
486 Moreno et al., 2015). Also shown in Figure 4 are the corresponding computed Br/OM ratio  
487 trends for both cores.

488 The FWCBr core presents Br concentrations in the range 129–560 mg/kg while the OM  
489 content varies between 4.9% and 23.6% (Appendix B), with values uniform from the base  
490 (AD 1190) until around AD 1920 (Br: 129–215 mg/kg; average  $161 \pm 5$  mg/kg; OM: 4.9–  
491 8.3%; average  $6.7 \pm 0.2\%$ ). Then, in the core's uppermost part, both Br and OM increase  
492 significantly, with two peaks at AD 1984 and AD 2010. This depth profile contrasts with the  
493 wider range and higher average Br content recorded in the FCPw1 core (Caminha):

494 average concentration of 747 mg/kg after the tidal marsh set up in AD 1330; minimum of 68  
495 mg/kg, AD 1143 and maximum of 1300 mg/kg by AD 1700 (Moreno et al., 2015). It seems  
496 important to mention the concomitant tidal marsh build-up in both places, as indicated by  
497 the core's analysis of preserved benthic foraminifera associations: AD 1330 in Caminha  
498 (Moreno et al., 2014) and AD 1323 in Casa Branca (unpublished data). This event occurs  
499 during the transition from the Medieval Climatic Anomaly (MCA; 900–1300) to the LIA  
500 (1350–1900) and it is likely related to the main MCA–LIA shifts in local-to-regional  
501 hydroclimatic conditions in Iberian Peninsula (e.g., Lebreiro et al., 2006; Moreno et al.,  
502 2012).

503 The strong direct Br–OM correlation identified in surface marsh environments is preserved  
504 in the cored sediment samples with depth ( $r= 0.91$ ;  $N= 30$ ;  $p < 0.001$ ), like previously  
505 described for the Caminha salt marsh ( $r= 0.83$ ;  $N= 49$ ;  $p < 0.001$ ). This Br–OM correlation  
506 occurs independently of the large differences observed between the two cores regarding  
507 their Br and OM inventories (Figure 4). Indeed, and despite the evidence provided herein  
508 showing that the Mira estuary is subject to greater influence from Br<sup>-</sup> enriched coastal  
509 waters than Minho, the FWCBBr core is relatively depleted in total Br (Appendix B). This  
510 depletion is also true for the amounts of long-term OM storage in both salt marshes  
511 soils/sediments. While in the FCPw1 core near 45% of the samples can be labelled as  
512 highly organic (OM > 30%) and *ca.* 41% as organic (organic content in the 15%–30%  
513 range), in the FWCBBr core almost 94% of the samples can be classified as mineral soils  
514 with organics (organic content > 3% and ≤ to 15%) (Huang et al., 2009). Therefore, and  
515 consistent with the Br–OM relationship (leading to the production of organobromine  
516 compounds) found in the surface/modern marsh habitats, it can be hypothesized that the  
517 primary driver of the whole dissimilar Br pool size of these two coastal tidal marshes is their  
518 technical C<sub>org</sub> sink capacity, constraining the amount of C<sub>org</sub> that is sequestered in each.  
519 Generally, decomposition rates in salt marshes are lower than OM inputs (allochthonous

520 and autochthonous), the reason why they are recognized as one of the most powerful C<sub>org</sub>  
521 sinks on the planet (e.g., Macreadie et al., 2013). However, it is expected that at a regional  
522 scale, soil/sediment C<sub>org</sub> pools are dependent upon several decomposition rate modifiers  
523 (e.g., litter chemical composition, climate, nutrient availability, communities of soil/sediment  
524 organisms, and site-specific factors), creating diverse geographic patterns as regards C<sub>org</sub>  
525 sequestration. Among those controls, salinity seems to be a major factor, and it is  
526 suggested that on tidal marshes soil C<sub>org</sub> sequestration increases with decreasing salinity  
527 (e.g., Poffenbarger et al., 2011; Van de Broek et al., 2016). Actually, salinity seems to have  
528 an even stronger impact than elevation on the soil/sediment OM pools of tidal marshes,  
529 inhibiting above-ground biomass and by enhancing OM mineralization (Hansen, 2015). In  
530 the climatic context of the Mira estuary, the evapotranspiration rates usually exceed  
531 precipitation, with tidal seawater supplying most of the moisture to the Casa Branca salt  
532 marsh soils/sediments. This induces high salinity even on the high marsh (Table 1), with  
533 Fatela et al. (2016) referring the occurrence of modern hypersaline conditions, with maxima  
534 records of 48‰, in the Mira lower estuary. Foraminiferal evidence (that will be discussed  
535 elsewhere) supports the idea that the (higher) Mira salinity baseline has been dominant  
536 across the timeframe investigated, with assemblages dominated by *Jadammina*  
537 *macrescens* (Brady, 1870) and *Trochammina inflata* (Montagu, 1808) (average 92%)  
538 (unpublished data). Such high salinity baseline is, in turn, a possible explanation to the  
539 lower OM in-depth concentrations from the FWCB<sub>r</sub> profile, which agrees with results from  
540 other studies (e.g., Van de Broek et al., 2016 and references therein).

541 Moreover, climate has a fundamental influence on the quantity (and quality) of inputs to the  
542 soil OM pool, with C<sub>org</sub> stocks being largest toward cooler and wetter locations, and smallest  
543 at hotter and drier regions, as established by other studies of terrestrial ecosystems (e.g.,  
544 Jenny, 1941; Meentemeyer, 1978; Liu et al., 2012, and references therein). These climatic  
545 gradients can have left their signature on the temporal evolution of the C<sub>org</sub> storage in the

546 Caminha and Casa Branca study sites. This is revealed by their individual temporal  
547 soil/sediment OM patterns, developed in response to the long-term climatic gradient  
548 between the NW and SW coasts of rising temperature and decreasing precipitation (as can  
549 be observed in Figure 4), with plausible direct implications on Br longer-time-scale trend, as  
550 explained before.

551 The strong direct Br–OM correlation holds for both the labile ( $r= 0.92$ ,  $N= 30$ ;  $p < 0.001$ ) and  
552 the relatively more recalcitrant OM ( $r= 0.88$ ;  $N= 30$ ;  $p < 0.001$ ) fractions from the Casa  
553 Branca salt marsh soils/sediments (results not shown). This result is consistent with recent  
554 investigation, in which a series of model experiments allowed to establish the existence of a  
555 natural, abiotic mechanistic source both of aliphatic (more labile) and aromatic (more  
556 recalcitrant) forms of  $Br_{org}$  in plant debris and humic substances in soil environment (Leri et  
557 al., 2014), and marine particulate OM (Leri and Ravel, 2015). The soil humic substances  
558 showed a recalcitrant aromatic  $Br_{org}$  speciation, leading Leri et al. (2014) to suggest that this  
559 might provide a useful proxy for evaluating the rate of OM burial in sediments. In this  
560 direction, is worth mentioning the work by Biester et al. (2004, 2006) and Martínez-Cortizas  
561 et al. (2007, 2016) in peatland soils, where they have started to study the temporal trends of  
562 the more stable  $Br_{org}$  compounds and the role of the main pedogenetic processes on Br  
563 accumulation. Altogether, this analysis can help future research on the Br–OM link in tidal  
564 marshes, needed to support the use of Br in marsh soils/sediments as a paleoclimatic  
565 indicator.

566 Finally, we propose a conceptual model for the salt marshes Br cycle in our case study  
567 (Caminha and Casa Branca) in order to summarize the interplay between the forcing factors  
568 analysed along the lines of the previous discussion. The interactions illustrated in Figure 5  
569 are, in our view, the most likely to have a strong influence on salt marshes short and even  
570 longer-term role to act as a source and/or as a sink for Br. Accordingly, NW coast high



571 marshes under the sustained influence of concomitant lower photosynthetically active  
572 radiation (PAR), corresponding to the spectral range of solar radiation from 400 to 700 nm  
573 that is used in photosynthesis reactions (e.g., Mariscal et al., 2000), and colder wetter  
574 conditions developed lower salinity baselines where the vegetation cover largely consists of  
575 non-succulents. These lower salinity (mesohaline) tidal marshes have typically higher rates  
576 of plant productivity and lower decomposition rates of dead and senescing plant material,  
577 leading to higher accumulation of soil/sediment OM (e.g., Morrissey et al., 2014).  
578 Collectively, these processes culminate in lesser CH<sub>3</sub>Br atmospheric emissions from  
579 marshes and higher Br<sub>org</sub> concentration in their soils/sediments. On the other hand, the SW  
580 coast high marshes, settled under higher available PAR conditions and a hotter and dryer  
581 climate, show a higher (polyhaline to euhaline) salinity baselines and consequently lower  
582 productivity, being mostly colonized by succulent plants more adapted to saline conditions  
583 and greater emitters of CH<sub>3</sub>Br. These conditions finally lead to a lower long-term storage of  
584 OM and Br<sub>org</sub> in soils/sediments.

585 The afore-described model establishes a connection with the analysis of the Br temporal  
586 variability in light of the past SA–climate link made in the next section.

587

### 588 *3.2.2. Br enrichment peaks in association with Grand Minima of solar activity*

589 The manifestation of a solar activity (SA) Grand Minima in terrestrial climate has been well  
590 established after the pioneering work of Eddy (1976). The most recent Grand Minima in  
591 reconstructed SA, as expressed by the TSI variation (Steinhilber et al., 2012), are presented  
592 in Figure 4 (Maunder Minimum – MM; 1645–1715; Spörer Minimum – SM; 1450–1550; and  
593 Wolf Minimum – WM; 1282–1342). Note that the Dalton Minimum (DM; 1790–1820) has a

594 distinct physical origin (Duhau and de Jager (2010), and it is therefore not regarded today  
595 as a Grand Episode of SA.

596 In the last few decades, extensive research work has been done towards a better  
597 understanding of the Sun-Earth's climate coupling system, with great progress being  
598 achieved (e.g., Haigh, 2007; Soon et al., 2014 for a review). Recently, Brugnara et al.  
599 (2013) referred that the Euro–Atlantic sector, in which Portugal is located, seems to be a  
600 region with a particularly strong solar influence on the troposphere, finding a weak but  
601 significant change in the mean late winter circulation over Europe, which culminates in  
602 detectable impacts on the near-surface climate. The results obtained by Jiang et al. (2015)  
603 suggest not only that climate in the northern North Atlantic regions follows SA fluctuations  
604 on multidecadal to centennial time scales, but also that it is more susceptible to the  
605 influence of those fluctuations throughout cool periods with, for instance, less vigorous  
606 ocean circulation. Similar results were found by Gómez-Navarro et al. (2012) in the context  
607 of climate simulations for the second millennium over the Iberian Peninsula. These  
608 researchers studied the impact of natural forcing and internal variability on climate, and  
609 found that temperature and precipitation variability are significantly affected at centennial  
610 scales by variations in the SA.

611 Grand Minima and Dalton-type Minimum scenarios are broadly characterized by (i) lower  
612 TSI (i.e., lower available PAR) (Lean, 1991, and references therein), (ii) development of  
613 cloudiness (e.g., Usoskin and Kovaltsov, 2008), and (iii) decreased global/regional air  
614 surface temperatures (e.g., Neukom et al., 2014) in tandem with greater regional  
615 precipitation variability. In the Iberian Peninsula, according with the modelled results from  
616 Gómez-Navarro et al. (2011), precipitation could have increased in response to reduced  
617 solar forcing (Figure 4), prompting greater river discharges. Also Cruz et al. (2015) related  
618 maxima rainfall episodes, as recognized in their stalagmite record, with other Grand Solar

619 Minima, suggesting a strong coupling between SA and precipitation over northern Iberia,  
620 which agrees with Gómez-Navarro et al. (2012) outcomes in the context of climate  
621 simulations.

622 Up to now, and in the absence of a “unified hypothesis”, the explanations for the  
623 connections between solar phenomena and the lower atmosphere processes can be  
624 summarized in two types of mechanisms: (i) “top-to-down”, influencing the pole-to-equator  
625 temperature gradient and exerting an impact on the modulation of the atmospheric  
626 circulation cells, weakening or strengthening the zonal winds, and (ii) “bottom-to-up” that  
627 directly impact on the radiation fluxes, energy balance and temperatures on the ground.  
628 Depending on the surface albedo a part of this radiation is absorbed and transformed into  
629 latent or sensible heat. During periods of lower SA, less radiation is available in the tropics  
630 for conversion to latent heat, which is thought to lead to a weakening of the Hadley and  
631 Ferrel cells (Labitzke et al., 2002). Other than intensity, the position and extent of those cells  
632 are also affected, inducing latitudinal shifts. Hence both mechanisms finally impact the  
633 atmospheric circulation modes responsible for the global/regional precipitation and  
634 temperature patterns (e.g., Gray et al., 2010; Martin-Puertas et al., 2012; Thiéblemont et al.,  
635 2015).

636 Therefore, if solar variations are an important source of regional climate variability, we might  
637 expect that paleoclimate proxies reproduce somewhat the climatic response to SA changes.  
638 In line with this, Moreno et al. (2015) suggested that Br soil/sediment enrichment in the  
639 Caminha salt marsh (NW coast) is, at least partially, related to the SA pattern over the last  
640 almost 800 years. This can be extended to Casa Branca salt marsh (SW coast), essentially  
641 through a SA control on (i) available PAR fluctuations and (ii) regional temperature and  
642 precipitation regimes, affecting evapotranspiration rates and, as a result, interstitial water  
643 salinity at the upper elevations within the marsh. Indeed, the relationship between the

644 curves presented in Figure 4 is clear, with periods of highest Br enrichment (FCPw1 and  
645 FWCBBr) agreeing with major excursions in SA. This means that the TSI negative anomalies  
646 (Steinhilber et al., 2012) from the Dalton, Maunder, Spörer and Wolf Solar Minima, to which  
647 correspond periods of both modelled lower temperature and increased precipitation in the  
648 NW and SW of Portugal (Gómez-Navarro et al., 2011), are marked by Br positive peaks in  
649 marshes soils/sediments, more clearly observed in Br/OM ratio curves to account for  
650 changes in OM content (see black arrows). Considering only the group of samples from the  
651 FWCBBr core falling within the LIA (with stronger impacts on the climate of Europe and other  
652 regions neighbouring the North Atlantic during the 16th–19th centuries; e.g., Mann, 2002),  
653 three display a more pronounced Br excess relative to OM, lying outside the upper 95%  
654 confidence limit of their linear regression interval: AD 1451 (Spörer Minimum), and AD 1694  
655 and AD 1660 (both in the Maunder Minimum). These sedimentary records, considered  
656 altogether with other climatic proxies for the NW of Portugal (Moreno et al., submitted),  
657 strongly suggest that the LIA resulted in a wetter and cool climate in this south-western  
658 European region, triggering major hydrological changes present in paleoecological records,  
659 namely from high marsh benthic foraminifera (Moreno et al., 2014). Specifically, climatic  
660 shifts driven by Grand Minima on western Portuguese coast could have forced a  
661 deceleration of the whole dynamics involving the net CH<sub>3</sub>Br phytogenic emissions to the  
662 atmosphere, thus favouring Br sequestration and storage (as Br<sub>org</sub>) in marsh  
663 soils/sediments. Throughout SA Grand Minima ( $\downarrow$ TSI/PAR), the climate controls departed  
664 from normal values ( $\downarrow$ T;  $\downarrow$ ET;  $\uparrow$ P; see Figure 5), inducing a decrease in marsh interstitial  
665 salinity, certainly ended in higher plant productivity peaks (e.g., De Leeuw et al., 1990),  
666 thereby causing a rise in salt marsh sediment C<sub>org</sub> accumulation over time, with plant debris  
667 more enriched in Br and liable to further bromination during the humification process.

668 Rhew et al. (2014) emphasized that CH<sub>3</sub>Br phytogenic emissions from coastal salt marshes,  
669 present a dramatic inter- and intra-marshes variability, namely in relation to magnitude

670 (subtropical salt marshes showing much higher emission rates than temperate salt  
671 marshes) and seasonality. They recorded maxima CH<sub>3</sub>Br emission fluxes in peak summer  
672 growing season (July) and lowest at the end of the growing season (November). The latter  
673 were registered during the morning and coincident with the high tide. They also found a  
674 pronounced mid-day peak, coinciding with the time of highest ambient air and surface soil  
675 temperatures, in the diurnal CH<sub>3</sub>Br emission trend, with this one mirroring the variation of  
676 PAR.

677 Considering both CH<sub>3</sub>Br phylogenetic emissions and the ubiquity of soil/sediment OM  
678 bromination, and applying them to a Grand Minima scenario (↓TSI/available PAR; ↓air  
679 surface temperatures; ↓growing seasons, ↑rainfall leading to ↑soil/sediment saturation), a  
680 reliable framework for the Br enrichment in temperate marsh habitats triggered by climatic  
681 shifts driven by SA can be proposed (see Figure 5), recognizing that further work would be  
682 required to completely prove this assumption.

683 Volcanic eruptions may also represent an alternative source of Br to salt marshes during  
684 Grand Minima Episodes (see Figure 4). The first discovery of volcanic BrO (Bobrowski et  
685 al., 2003), and its subsequent measurement in many volcanic plumes around the globe  
686 (e.g., Roberts et al., 2014) demonstrates the formation of reactive bromine (firstly as Br<sub>2</sub>,  
687 which then converts into other forms including Br, BrO, HOBr, BrONO<sub>2</sub>) during these  
688 events, which can be removed (at least partially) from gaseous phase by aerosol, water and  
689 ice-uptake (followed by particle sedimentation) (Fernandez et al., 2014; Jourdain et al.,  
690 2015). Reactive bromine acts as a catalyst to its own formation, leading to an exponential  
691 growth called “bromine explosion”. The LIA Grand Minima have been punctuated by  
692 considerable volcanic activity (e.g., D’Arrigo et al., 2013; Figure 4). D’Arrigo et al. (2013)  
693 highlighted, as two of the major volcanic events over the past millennium, the eruptions of  
694 AD 1453 (Kuwae Volcano, Vanuatu; Spörer Minimum) and AD 1815 (Mount Tambora,

695 Indonesia; Dalton Minimum). Such episodes of great volcanic activity and their worldwide  
696 effects (e.g., Trigo et al., 2009; Koffman et al., 2013) might also have had the potential for  
697 causing disruption on the Br cycling in Caminha and Casa Branca salt marshes, contributing  
698 somewhat for their soils/sediments Br enrichment throughout Grand Minima.

699

#### 700 **4. Conclusions**

701 The present study addresses major topics concerning the Br cycling in contrasting salt  
702 marshes environments of four western Portuguese estuaries – Minho, Lima, Sado and Mira,  
703 drawing attention for its complexity and linkages with OM dynamics. We provided evidence  
704 that besides the marine influence, Br enrichment of these marshes is ultimately connected  
705 to their ability for long-term  $C_{org}$  storage. A clear difference between the marshes from NW  
706 and SW coasts stands out, with the former being more enriched in both OM and total Br.  
707 This contrasting behaviour is driven by different climatic conditions between the two regions  
708 that favour more strongly the mechanisms and processes of OM production, burial, and  
709 preservation (with concomitant incorporation of Br) in the north-western coastal salt  
710 marshes, in contrast with the SW coast, most probably as a result of the higher salinity  
711 (lesser productivity) of the latter. Seemingly, this same NW climatic setting inhibits the  
712 emission of comparatively larger phytogetic  $CH_3Br$  fluxes to atmosphere. This might be  
713 intensified as a result of the marshes colonization by non-succulent species (less efficient in  
714 the  $CH_3Br$  production), further promoting the Br enrichment of soil/sediment OM.

715 Although the applied approach is constrained by chronological uncertainties, cores sampling  
716 resolution or the (relatively short) time series lengths, preventing the application of  
717 enhanced methodologies in the time-frequency domain, the Br temporal variability in the  
718 Caminha and Casa Branca salt marshes can be related to SA oscillations, showing greater

719 Br enrichment during Grand Minima or Minima-like Episodes. This can be explained in  
720 connection with the changing temperature (decrease) and precipitation (increase) regimes  
721 in the NW and SW coasts of Portugal induced by lower TSI (available PAR), as pointed out  
722 by previous studies and supported by climate simulations. The contribution of major tropical  
723 volcanic explosions at Grand Solar Minima during the registered higher Br enrichment in the  
724 two Portuguese salt marshes is also considered.

725 Finally, we expect that the issues encompassed here can be deepened in future research  
726 about the Br biogeochemical cycle in salt marshes worldwide. The proposed conceptual  
727 framework identifies several influences capable of imbalance the Br–OM interconnections  
728 and helps to prioritize which are likely to play key roles on salt marshes Br recycling, in  
729 order to improve, henceforward, its reliability as a marker of climate change driven by past  
730 SA. In line with this, it is important to bear in mind that for robustly test solar-climate signals  
731 in Br tidal salt marsh records, large and widespread ensembles of well-dated data are  
732 required along with high-resolution sampling.

733

## 734 **Acknowledgements**

735 This work was partly supported by IDL through the UID/GEO/50019/2013 program, by C<sup>2</sup>TN  
736 through the UID/Multi/04349/2013 program, and is a contribution of the project WestLog  
737 (PTDC/CTE/105370/2008), funded by the Fundação para a Ciência e a Tecnologia (FCT).  
738 João Moreno benefits from a FCT PhD grant (SFRH/BD/ 87995/2012). The authors would  
739 like to express their sincere gratitude to Inês Pereira, Ana Medeiros and Vera Lopes for  
740 carrying out the soils and sediments geochemical analysis, and the proof-reader Carla  
741 Neves. J.J. Gómez-Navarro acknowledges the funding provided through the contract for the  
742 return of experienced researches, resolution R-735/2015 of the University of Murcia.

743

744 **References**

745

746 Adam, P., 1990. Salt marsh ecology. Cambridge University Press, Cambridge, UK, 461p.

747

748 Adams, S.S., 1969. Bromine in the Salado Formation, Carlsbad Potash District, New  
749 Mexico. State Bureau of Mines and Mineral Resources, Bulletin 93, Socorro, New Mexico,  
750 122 p.

751

752 Adolphi, F. and Muscheler, R., 2016. Synchronizing the Greenland ice core and radiocarbon  
753 timescales over the Holocene – Bayesian wiggle-matching of cosmogenic radionuclide  
754 records. *Climate of the Past* 12, 15–30.

755

756 Alcalá, F.J. and Custodio, E., 2008. Using the Cl/Br ratio as a tracer to identify the origin of  
757 salinity in aquifers in Spain and Portugal; *Journal of Hydrology* 359, 189–207.

758

759 Almeida, C.M.R., Mucha, A.P. and Vasconcelos, M.T., 2011. Role of different salt marsh  
760 plants on metal retention in an urban estuary (Lima estuary, NW Portugal). *Estuarine,  
761 Coastal and Shelf Science* 91, 243–249.

762

763 Alves, A.M.C., 2003. O estuário do rio Lima: pressão antrópica e caracterização ambiental.  
764 *Ciências da Terra (UNL)*, Lisboa, special nº. V, CD-ROM, pp. H5–H9.

765

766 Amaral, V., Queiroga, H., Skov, M. and Paula, J., 2007. Planktonic availability and  
767 settlement of *Carcinus maenas megalopae* at high temporal resolution in the lower Mira  
768 Estuary (SW Portugal). *Marine Ecology Progress Series* 348, 239–248.



769

770 APA, 2011. Sistema Nacional de Informação de Ambiente da Agência Portuguesa do  
771 Ambiente (SNIAmb).<http://sniamb.apambiente.pt/>.

772

773 Appleby, P.G., 2001. Chronostratigraphic techniques in recent sediments. *In* W.M. Last, J.P.  
774 Smol (Eds.), *Tracking Environmental Change Using Lake Sediments*, 1. Dordrecht, The  
775 Netherlands: Kluwer Academic Publishers, p. 171–203.

776

777 Appleby, P.G. and Oldfield, F., 1978. The calculation of lead-210 dates assuming a constant  
778 rate of supply of unsupported  $^{210}\text{Pb}$  to the sediment. *Catena* 5, 1–8.

779

780 Araújo, M.F., Valério, P. and Jouanneau, J-M., 1998. Heavy metal assessment in sediments  
781 of the Ave river basin (Portugal) by EDXRF. *X-Ray Spectrometry* 27, 305–312.

782

783 Araújo, M.F., Conceição, A., Barbosa, T., Lopes, M.T. and Humanes, H. 2003. Elemental  
784 composition of marine sponges from the Berlengas Natural Park, Western Portuguese  
785 Coast. *X-Ray Spectrometry* 32, 428–433.

786

787 Azevedo, I., Ramos, S., Mucha, A.P. and Bordalo, A.A., 2013. Applicability of ecological  
788 assessment tools for management decision-making: A case study from the Lima estuary  
789 (NW of Portugal). *Ocean & Coastal Management* 72, 54–63.

790

791 Bettencourt, A., Ramos, L., Gomes, V., Dias, J.M.A., Ferreira, G., Silva, M. and Costa, L.,  
792 2003. *Estuários Portugueses*. Ed. INAG – Ministério das Cidades, Ordenamento do  
793 Território e Ambiente, Lisboa, 311 p.

794

795 Biester, H., Keppler, F., Putschew, A., Martínez-Cortizas and Petri, M., 2004. Halogen  
796 retention, organohalogens, and the role of organic matter decomposition on halogen  
797 enrichment in two Chilean peat bogs. *Environmental Science & Technology* 38, 1984–1991.  
798

799 Biester, H., Selimović, D., Hemmerich, S., and Petri, M., 2006. Halogens in pore water of  
800 peat bogs – the role of peat decomposition and dissolved organic matter. *Biogeosciences* 3,  
801 53–64.  
802

803 Blei, E., Heal, M.R. and Heal, K.V., 2010. Long-term CH<sub>3</sub>Br and CH<sub>3</sub>Cl flux measurements  
804 in temperate salt marshes. *Biogeosciences* 7, 3657–3668.  
805

806 Bobrowski, N., Hönninger, G., Galle, B. and Platt, U., 2003. Detection of bromine monoxide  
807 in a volcanic plume, *Nature*, 423, 273–276.  
808

809 Boorman, L.A., 2003. *Saltmarsh Review. An overview of coastal saltmarshes, their dynamic  
810 and sensitivity characteristics for conservation and management.* JNCC Report, No. 334,  
811 113p.  
812

813 Bridgham, S.D., Megonigal, J.P., Keller, J.K., Bliss, N.B. and Trettin, C., 2006. The carbon  
814 balance of North American wetlands. *Wetlands* 26, 889–916.  
815

816 Brugnara, Y., Brönnimann, S., Luterbacher, J. and Rozanov, E., 2013. Influence of the  
817 sunspot cycle on the Northern Hemisphere wintertime circulation from long upper-air data  
818 sets. *Atmospheric Chemistry and Physics* 13, 6275–6288.  
819

820 Buchanan, J.B. and Longbottom, M.R., 1970. The determination of organic matter in marine  
821 muds: the effect of the presence of coal and the routine determination of protein. *Journal of*  
822 *Experimental Marine Biology and Ecology* 5, 158–169.

823

824 Cardoso, R., Araújo, M.F., Freitas, M.C. and Fatela, F., 2008. Geochemical characterisation  
825 of sediments from marginal environments of Lima Estuary (NW Portugal). *e-Terra, Revista*  
826 *Electrónica de Ciências da Terra* Volume 5 – Nº 6, GEOTIC – Sociedade Geológica de  
827 Portugal, 11 p.

828

829 Carpenter, L.J. and Reimann, S. (Lead Authors), Burkholder, J.B., Clerbaux, C., Hall, B.D.,  
830 Hossaini, R., Laube, J.C., and Yvon Lewis, S.A., 2014. Ozone-Depleting Substances  
831 (ODSs) and Other Gases of Interest to the Montreal Protocol. Chapter 1 in *Scientific*  
832 *Assessment of Ozone Depletion: 2014, Global Ozone Research and Monitoring Project-*  
833 *Report Nº 55, World Meteorological Organization, Geneva, Switzerland.*

834

835 Castro, P. and Freitas, H., 2006. Anthropogenic effects and salt marsh loss in the Mondego  
836 and Mira estuaries (Portugal). *Web Ecology* 6, 59–66.

837

838 Chipperfield, M.P., 2015. Global Atmosphere – The Antarctic Ozone Hole. *In Still Only One*  
839 *Earth: Progress in the 40 Years since the First UN Conference on the Environment, 2015,*  
840 *pp. 1–33.*

841

842 Correns, C.W., 1956. The Geochemistry of Halogens. *In* L.H. Ahrens, K. Rankama and S.K.  
843 Rancorn (Eds.), *Physics and Chemistry of the Earth, Vol. 1, Pergamon Press, New York,*  
844 *pp. 181–233.*

845

846 Costa, M.J. Catarino, F. and Bettencourt, A., 2001. The role of salt marshes in the Mira  
847 estuary (Portugal). *Wetlands Ecology and Management* 9, 121–134.

848

849 Costa, J.C., 2001. Tipos de vegetação e adaptações das plantas do litoral de Portugal  
850 continental. *In* M.E. Albergaria Moreira, A. Casal Moura, H.M. Granja and F. Noronha (Eds.)  
851 Homenagem (in honorio) Professor Doutor Soares de Carvalho. Universidade do Minho,  
852 Braga, pp. 283–299.

853

854 Costa, J.C., Arsénio, P., Monteiro-Henriques, T., Neto, C., Pereira, E., Almeida, T. and Izco,  
855 J., 2009. Finding the boundary between Eurosiberian and Mediterranean salt marshes.  
856 *Journal of Coastal Research* SI 56, 1340–1344.

857

858 Costa-Dias, S., Ronaldo Sousa, R. and Antunes, C., 2010. Ecological quality assessment of  
859 the lower Lima Estuary. *Marine Pollution Bulletin* 61, 234–239.

860

861 Cox, M.L., Fraser, P.J., Sturrock, G.A., Siems, S.T. and Porter, L.W., 2004 Terrestrial  
862 sources and sinks of halomethanes near Cape Grim, Tasmania. *Atmospheric Environment*  
863 38, 3839–3852.

864

865 Crowley, T.J., 2000. Causes of climate change over the past 1000 years. *Science* 289,  
866 270–277.

867

868 Cruz, J.A., Turrero, M.J., Cáceres, J.O., Marín-Roldán, A., Ortega, A.I., Garralón, A.,  
869 Sánchez. L., Gómez, P., Muñoz-García, M.B., Edwards, R.L. and J. Martín-Chivelet, J.,  
870 2015. Long-term hydrological changes in northern Iberia (4.9–0.9 ky BP) from speleothem

871 Mg/Ca ratios and cave monitoring (Ojo Guarenã Karst Complex, Spain) *Environmental*  
872 *Earth Sciences* 74, 7741–7753.

873

874 Cundy, A.B., Hopkinson, L., Lafite, R., Spencer, K., Taylor, J.A., Ouddane, B., Heppell,  
875 C.M., Carey, P.J., Charman, R.O., Shell, D., Ulliyott, J.S., 2005. Heavy metal distribution  
876 and accumulation in two *Spartina* sp.-dominated macrotidal salt marshes from the Seine  
877 estuary (France) and the Medway estuary (UK). *Applied Geochemistry* 20, 1195–1208.

878

879 Cunha, A.H., Assis, J.F. and Serrão, E.A., 2013. Seagrasses in Portugal: a most  
880 endangered marine habitat. *Aquatic Botany* 104, 193–203.

881

882 D'Arrigo, R., Wilson, R. and Anchukaitis, K.J., 2013. Volcanic cooling signal in tree ring  
883 temperature records for the past millennium. *Journal of Geophysical Research:*  
884 *Atmospheres* 118, 1–11.

885

886 De Leeuw, J., Olf, H. and Bakker, J.P., 1990. Year-to-year variation in peak above-ground  
887 biomass of six salt-marsh angiosperm communities as related to rainfall deficit and  
888 inundation frequency. *Aquatic Botany* 36, 139–151.

889

890 Dimmer, C.H., Simmonds, P.G., Nickless, G. and Nickless, M.R., 2000. Biogenic fluxes of  
891 halomethanes from Irish peatland ecosystems. *Atmospheric Environment* 35, 321–330.

892

893 Doff, D.H., 1989. Determination of bromine and iodine in four marine sediment reference  
894 samples by Energy-Dispersive X-Ray Fluorescence Spectrometry. *Geostandards*  
895 *Newsletter* 13, 75–77.

896

897 Drewer, J., Heal, M.R., Heal, K.V. and Smith, K.A., 2006. Temporal and spatial variation in  
898 methyl halide flux from a salt marsh. *Geophysical Research Letters* 33, L16808, 5 p.  
899

900 Duhau, S., and De Jager, C., 2010. The forthcoming Grand Minimum of solar activity,  
901 *Journal of Cosmology* 8, 1983-1999.  
902

903 Eddy, J.A., 1976. The Maunder Minimum. *Science* 192, 1189–1202.  
904

905 Fagherazzi, S., Wiberg, P.L., Temmerman, S., Struyf, E., Zhao, Y. and Raymond, P.A.,  
906 2013. Fluxes of water, sediments, and biogeochemical compounds in salt marshes.  
907 *Ecological Processes* 2, 1–16.  
908

909 Fatela, F., Moreno, J. and Cabral, M.C., 2016. Salinity and temperature water assessment  
910 of the tidal marshes from the W Portuguese coast, as an ecological tool to  
911 palaeoenvironmental reconstructions based on foraminifera and ostracoda assemblages.  
912 *Estudos do Quaternário*, 14, <http://www.apeq.pt/ojs/index.php/apeq>.  
913

914 Fatela, F., Moreno, J., Moreno, F., Araújo, M.F., Valente, T., Antunes, C., Taborda, R.,  
915 Andrade, C., Drago, T., 2009. Environmental constraints of foraminiferal assemblages  
916 distribution across a brackish tidal marsh (Caminha, NW Portugal). *Marine*  
917 *Micropaleontology* 70, 70–88.  
918

919 Fatela, F., Moreno, J. and Antunes, C., 2007. Salinity influence on foraminiferal tidal marsh  
920 assemblages of NW Portugal: an anthropogenic constraint? *Thalassas* 23, 51–63.  
921

922 Fernandez, R.P., Salawitch, R.J., Kinnison, D.E., Lamarque, J.-F. and Saiz-Lopez, A., 2014.  
923 Bromine partitioning in the tropical tropopause layer: implications for stratospheric injection.  
924 *Atmospheric Chemistry and Physics* 14, 13391–13410.

925

926 Ferreira, J.G., Simas, T., Nobre, A., Silva, M.C., Shifferegger, K. and Lencart-Silva, J.,  
927 2003. Identification of sensitive areas and vulnerable zones in transitional and coastal  
928 Portuguese systems. INAG, Lisboa, 151 p.

929

930 Flury, M. and Papritz, A., 1993. Bromide in the natural environment: occurrence and toxicity.  
931 *Journal of Environmental Quality* 22, 747–758.

932

933 Gerlach, A., 1999. Winter driftline debris on the Wadden Island of Mellum, Germany;  
934 distribution, quantity and decomposition. *Abhandlungen Naturwissenschaftliches Verein*  
935 *Bremen* 44, pp. 707–724.

936

937 Gerritse, R.G. and George, R., 1988. The role of soil organic matter in the geochemical  
938 cycling of chloride and bromide. *Journal of Hydrology* 101, 83–95.

939

940 Gettner, S., 2003. Untersuchungen des Zusammenhangs zwischen Treibselmengen und  
941 Vorlandnutzung an der Westküste Schleswig-Holsteins. *Kieler Notizen Pflanzenkunde*  
942 *Schleswig Holstein Hamburg* 31, pp. 57–71.

943

944 Gómez-Navarro, J.J., Montávez, J.P., Jiménez-Guerrero, P., Jerez, S., Lorente-Plazas, R.,  
945 González-Rouco, J.F. and Zorita, E., 2012. Internal and external variability in regional  
946 simulations of the Iberian Peninsula climate over the last millennium. *Climate of the Past* 8,  
947 25–36.

948

949 Gómez-Navarro, J.J., Montávez, J.P., Jerez, S., Jiménez-Guerrero, P., Lorente-Plazas, R.,  
950 González-Rouco, J.F. and Zorita, E., 2011. A regional climate simulation over the Iberian  
951 Peninsula for the last millennium. *Climate of the Past* 7, 451–472.

952

953 Gontikaki, E., Thornton, B., Huvenne, V.A.I. and Witte, U., 2013. Negative priming effect on  
954 organic matter mineralisation in NE Atlantic slope Sediments. *PLoS ONE* 8(6): e67722, 9 p.

955

956 Gray, L.J, Beer, J., Geller, M., Haigh, J.D., Lockwood, M., Matthes, K., Cubasch, U.,  
957 Fleitmann, D., Harrison, G., Hood, L., Luterbacher, J., Meehl, G.A., Shindell, D., van Geel,  
958 B. and White, W. 2010. Solar influences on climate. *Reviews of Geophysics* 48, RG4001,  
959 53 p.

960

961 Haigh, J.D., 2007. The sun and the earth's climate. *Living Review Solar Physics* 4, 1e64  
962 (Online article). Available at: <http://www.livingreviews.org/lrsp-2007-2> (accessed  
963 08.05.2016).

964

965 Hamilton, J., McRoberts W., Keppler, F., Kalin, R. and Harper, D., 2003. Chloride  
966 methylation by plant pectin: An efficient environmentally significant process, *Science* 301,  
967 206–209.

968

969 Hansen, K., 2015. Ecosystem functions of tidal marsh soils of the Elbe estuary. Dissertation,  
970 Fachbereich Geowissenschaften, Universität Hamburg, Hamburger Bodenkundliche  
971 Arbeiten 76, XX + 161p.

972



973 Hardacre, C.J. and Heal, M.R., 2013. Characterization of methyl bromide and methyl  
974 chloride fluxes at temperate freshwater wetlands. *Journal of Geophysical Research:*  
975 *Atmospheres* 118, 977–991.

976

977 Hardacre, C.J., Blei, E. and Heal, M.R., 2009. Growing season methyl bromide and methyl  
978 chloride fluxes at a sub-arctic wetland in Sweden. *Geophysical Research Letters* 36,  
979 L12401, 5 p.

980

981 Haslett, J. and Parnell, A., 2008. A simple monotone process with application to  
982 radiocarbon-dated depth chronologies. *Applied Statistics* 57, 399–418.

983

984 Herbst, K., Heber, B., Beer, J. and Tylka, A.T., 2015. Modelling the Production of  
985 Cosmogenic Radionuclides due to galactic and solar cosmic rays. *The 34th International*  
986 *Cosmic Ray Conference, PoS (ICRC2015) 537, 8p.*

987

988 Honrado, J., Alves, P., Alves, H.N., Torres, J. and Caldas, F.B., 2004. A Flora e a  
989 vegetação do Minho internacional – Diversidade, ecologia e valor para conservação.  
990 *Melgaço, Portugal: Atas do Congresso Internacional Sobre o Rio Minho; 5p.*

991

992 Hu, L., Yvon-Lewis, S.A., Liu, Y., Salisbury, J.E. and O'Hern, J.E., 2010. Coastal emissions  
993 of methyl bromide and methyl chloride along the eastern Gulf of Mexico and the east coast  
994 of the United States. *Biogeochemical Cycles* 24, GB1007, 10 p.

995

996 Huang, P.-T., Patel, M., Santagata, M.C., and Bobet, A., 2009. Classification of organic  
997 soils. FHWA/IN/JTRP-2008/2. Purdue University, 170 p.

998

999 Hurrell, J., 1995. Decadal trends in the North-Atlantic Oscillation: regional temperatures and  
1000 precipitation. *Science* 269, 676–679.

1001

1002 Hurrell, J. and van Loon, H., 1997. Decadal variations in climate associated with the North  
1003 Atlantic Oscillation. *Climatic Change* 36, 301–336.

1004

1005 Jenny, H., 1941. *Factors of Soil Formation - A System of Quantitative Pedology*. Dover  
1006 Publications, Inc., New York, 291 p.

1007

1008 Jiang, H., Muscheler, R., Björck, S., Seidenkrantz, M.-S., Olsen, J., Sha, L., Sjolte, J.,  
1009 Eiríksson, J., Ran, L., Knudsen, K.-L., and Knudsen, M.F., 2015. Solar forcing of Holocene  
1010 summer sea-surface temperatures in the northern North Atlantic. *Geology*  
1011 doi:10.1130/G36377.1.

1012

1013 Jones, F., Vengosh, A., Rosenthal, E., Yechieli, Y., 1999. Geochemical investigation of  
1014 groundwater quality. In: *Proceeding: Seawater Intrusion in Coastal Aquifers - Concepts,*  
1015 *Methods and Practices*. Kluwer Academic, Dordrecht, pp. 51–71.

1016

1017 Jourdain, L., Roberts, T.J., Pirre, M. and Josse, B., 2015. Modeling the reactive halogen  
1018 plume from Ambrym volcano and its impact on the troposphere with the CCATT-BRAMS  
1019 mesoscale model. *Atmospheric Chemistry and Physics Discuss.* 15, 35313–35381.

1020

1021 Katz, B.G., Eberts, S.M. and Kauffman, L.J., 2011. Using Cl/Br ratios and other indicators to  
1022 assess potential impacts on groundwater quality from septic systems: A review and  
1023 examples from principal aquifers in the United States. *Journal of Hydrology* 397, 151–166.

1024

1025 Keene, W.C., Stutz, J., Pszenny, A.A.P., Maben, J.R., Fischer, E.V., Smith, A.M., von  
1026 Glasow, R., Pechtl, S., Sive, B.C. and Varner, R.K., 2007. Inorganic chlorine and bromine in  
1027 coastal New England air during summer. *Journal of Geophysical Research* 112, D10S12,  
1028 15 p.

1029

1030 Keller, J.K., Bauers, A.K., Bridgham, S.D., Kellogg, L.E. and Iversen, C.M., 2006. Nutrient  
1031 control of microbial carbon cycling along an ombrotrophic-minerotrophic peatland gradient,  
1032 *Journal of Geophysical Research* 111, G03006, 14 p.

1033

1034 Keppler, F., Eiden, R., Niedan, V., Pracht, J., and Scholer, H.F., 2000. Halocarbons  
1035 produced by natural oxidation processes during degradation of organic matter, *Nature* 403,  
1036 298–301.

1037

1038 Keppler, F., Kalin, R.M., Harper, D.B., McRoberts, W.C. and Hamilton, J.T.G., 2004. Carbon  
1039 isotope anomaly in the major plant C1 pool and its global biogeochemical implications,  
1040 *Biogeosciences* 1, 123–131.

1041

1042 Koffman, B.G., Kreutz, K.J., Kurbatov, A.V. and Dunbar, N.W., 2013. Impact of known local  
1043 and tropical volcanic eruptions of the past millennium on the WAIS Divide microparticle  
1044 record. *Geophysical Research Letters* 40, 4712–4716.

1045

1046 Koh, D.-C., Mayer, B., Lee, K.-S. and Ko, K.-S., 2010. Land-use controls on sources and  
1047 fate of nitrate in shallow groundwater of an agricultural area revealed by multiple  
1048 environmental tracers. *Journal of Contaminant Hydrology* 118, 62–78.

1049

1050 Kristensen, E., 1990. Characterization of biogenic organic matter by stepwise  
1051 thermogravimetry (STG). *Biogeochemistry* 9, 135–159.

1052

1053 Labitzke, K., Austin, J., Butchart, N., Knight, J., Takahashi, M., Nakamoto, M., Nagashima,  
1054 T., Haigh, J., and Williams, V., 2002. The global signal of the 11-year solar cycle in the  
1055 stratosphere: observations and models, *Journal of Atmospheric and Solar-Terrestrial*  
1056 *Physics* 64, 203–210.

1057

1058 Lal, D. and Peters, B., 1967. Cosmic ray produced radioactivity on the Earth. *In* K. Sitte  
1059 (Ed.), *Handbuch der Physik / Encyclopedia of Physics*, vol. 9 / 46 / 2, Springer-Verlag,  
1060 Berlin, pp. 551–612.

1061

1062 Lean J., 1991. Variations in the sun's radiative output. *Reviews of Geophysics* 29, 505–535.

1063

1064 Lebreiro, S.M., Francés, S.G., Abrantes, F.F.G., Diz, P., Bartels-Jónsdóttir, H.B.,  
1065 Stroynowski, Z.N., Gil, I.M., Pena, L.D., Rodrigues, T., Jones, P.D., Nombela, M.A., Alejo, I.,  
1066 Briffa, K.R., Harris, I. and Grimalt, J.O., 2006. Climate change and coastal hydrographic  
1067 response along the Atlantic Iberian margin (Tagus Prodelta and Muros Ría) during the last  
1068 two millennia. *The Holocene* 16, 1003–1015.

1069

1070 Lefeuvre, J.-C., Bouchard, V., Feunteun, E., Grare, S., Laffaille, P. and Radureau, A., 2000.  
1071 European salt marshes diversity and functioning: the case study of the Mont Saint-Michel  
1072 bay, France. *Wetland Ecology and Management* 8, 147–161.

1073

1074 Leorri, E., Freitas, M.C., Zourarah, B., Andrade, C., Mellas, S., Cruces, A., Griboulard, R.  
1075 and Lopes, V., 2010. Multiproxy approach to characterize an overwash deposit: Oualidia  
1076 lagoon (Moroccan Atlantic coast). *GEOGACETA* 48, 7–10.

1077

1078 Leri, A.C. and Ravel, B., 2015. Abiotic bromination of soil organic matter. *Environmental*  
1079 *Science & Technology* 49, 13350–13359.

1080

1081 Leri, A.C., Mayer, L.M., Thornton, K.R. and Ravel, B., 2014. Bromination of marine  
1082 particulate organic matter through oxidative mechanisms. *Geochimica et Cosmochimica*  
1083 *Acta* 142, 53–63.

1084

1085 Leri, A.C. and Myneni, S.C.B., 2012. Natural organobromine in terrestrial ecosystems.  
1086 *Geochimica and Cosmochimica Acta* 77, 1–10.

1087

1088 Leri, A.C., Hakala, J.A., Marcus, M.A., Lanzirotti, A., Reddy, C.M. and Myneni, S.C.B., 2010.  
1089 Natural organobromine in marine sediments: new evidence of biogeochemical Br cycling.  
1090 *Global Biogeochemical Cycles* 24, GB4017, 15 p.

1091

1092 Lewis, D.B., Brown, J.A. and Jimenez, K.L., 2014. Effects of flooding and warming on soil  
1093 organic matter mineralization in *Avicennia germinans* mangrove forests and *Juncus*  
1094 *roemerianus* salt marshes. *Estuarine, Coastal and Shelf Science* 139, 11–19.

1095

1096 Lima, I., Moreira, S.M., Osten, JR.-V., Soares, A.M.V.M. and Guilhermino, L., 2007.  
1097 Biochemical responses of the marine mussel *Mytilus galloprovincialis* to petrochemical  
1098 environmental contamination along the North-western coast of Portugal. *Chemosphere* 66,  
1099 1230–1242.

1100

1101 Liu, Z.P., Shao, M.A. and Wang, Y.Q., 2012. Large-scale spatial variability and distribution  
1102 of soil organic carbon across the entire Loess Plateau, China. *Soil Research* 50, 114–124.

1103

1104 Macreadie, P.I., Hughes, A.R. and Kimbro, D.L., 2013. Loss of “blue carbon” from coastal  
1105 salt marshes following habitat disturbance. *PLoS ONE* 8, e69244, 8 p.

1106

1107 Mahn, C.L. and Gieskes J.M., 2001. Halide systematics in comparison with nutrient  
1108 distributions in sites 1033B and 1034B, Saanich Inlet: ODP Leg 169S. *Marine Geology* 174,  
1109 323–339.

1110

1111 Manley, S.L., Wang, N.-Y., Walser, M.L., and Cicerone, R.J., 2006. Coastal salt marshes as  
1112 global methyl halide sources from determinations of intrinsic production by marsh plants.  
1113 *Global Biogeochemical Cycles* 20, GB3015, 13 p.

1114

1115 Mann, M.E., Zhang, Z., Rutherford, S., Bradley, R.S., Hughes, M.K., Shindell, D., Ammann,  
1116 C., Faluvegi, G. and Ni, F., 2009. Global signatures of the Little Ice Age and Medieval  
1117 climate anomaly and plausible dynamical origins, *Science* 326, 1256–1260.

1118

1119 Mayer, L.M., 1994. Relationships between mineral surfaces and organic carbon  
1120 concentrations in soils and sediments. *Chemical Geology* 114, 347–363.

1121

1122 Mayer, L.M., Schick, L.L., Allison, M.A., Ruttenberg, K.C. and Bentley, S.J., 2007. Marine  
1123 vs. terrigenous organic matter in Louisiana coastal sediments: The uses of bromine:organic  
1124 carbon ratios. *Marine Chemistry* 107, 244–254.

1125

1126 Mariscal, M.J., Orgaz, F. and Villalobos, F.J., 2000. Modelling and measurement of  
1127 radiation interception by olive canopies. *Agricultural and Forest Meteorology* 100,183–197.  
1128

1129 Marques, B., Lillebø A.I., Pereira, E. and Duarte, A.C., 2011. Mercury cycling and  
1130 sequestration in salt marshes sediments: An ecosystem service provided by *Juncus*  
1131 *maritimus* and *Scirpus maritimus*. *Environmental Pollution* 159, 1869–1876.  
1132

1133 Martin-Puertas, C., Matthes, K., Brauer, A., Muscheler, R., Hansen, F., Petrick, C., Aldahan,  
1134 A., Possnert, G. and van Geel, B., 2012. Regional atmospheric circulation shifts induced by  
1135 a grand solar minimum. *Nature Geoscience* 5, 397–401.  
1136

1137 Martínez-Cortizas, A., Vázquez, C.F., Kaal, J., Biester, H., Casais, M.C., Rodríguez, T.T.  
1138 and Lado, L.R., 2016. Bromine accumulation in acidic black colluvial soils. *Geochimica et*  
1139 *Cosmochimica Acta* 174, 143–155.  
1140

1141 Martínez-Cortizas, A., Biester, H., Mighall, T. and Bindler, R., 2007. Climate-driven  
1142 enrichment of pollutants in peatlands. *Biogeosciences* 4, 905–911.  
1143

1144 Martins, F., Leitão, P., Silva, A. and Neves, R., 2001. 3D modelling in the Sado estuary  
1145 using a new generic vertical discretization approach. *Oceanologica Acta* 24, 1–12.  
1146

1147 Masarik, J. and Beer, J., 1999. Simulation of particle fluxes and cosmogenic nuclide  
1148 production in the Earth's atmosphere. *Journal of Geophysical Research* 104, 12099–12111.  
1149

1150 Meentemeyer, V., 1978. Macroclimate and lignin control of litter decomposition rates.  
1151 *Ecology* 59, 465–472.

1152

1153 Millero, F.J., 2013. Chemical Oceanography, CRC Press, 4<sup>th</sup> edition, Boca Raton, 571 p.

1154

1155 Mineke, W. and Bakker, J.P., 2002. Soil seed bank and driftline composition along a  
1156 successional gradient on a temperate salt marsh. *Applied Vegetation Science* 5, 55–62.

1157

1158 Moreira, M.E.S.A., 1992. Recent saltmarsh changes and sedimentation rates in the Sado  
1159 estuary, Portugal. *Journal of Coastal Research* 8, 631–640.

1160

1161 Moreno, A., Pérez, A., Frigola, J., Nieto-Moreno, V., Rodrigo-Gámiz, M., González-  
1162 Sampériz,

1163 P., Morellón, M., Martín-Puertas, C., Corella, J.P., Belmonte, Á., Sancho, C., Cacho, I.,

1164 Herrera, G., Canals, M., Jiménez-Espejo, F., Martínez-Ruiz, F., Vegas, T. and Valero

1165 Garcés,

1166 B.L., 2012. The Medieval Climate Anomaly in the Iberian Peninsula reconstructed from  
1167 marine and lake records. *Quaternary Science Reviews* 43, 16–32.

1168

1169 Moreno, J., Fatela, F., M.A. Gonçalves, M.A., Leorri, E., Gómez-Navarro, J.J., Brázdil, R.,

1170 Ferreira, M.J., Moreno, F. and R. Trigo (submitted). A bi-proxy paleoclimatic reconstruction

1171 for the Entre-Douro-e-Minho region, northwest Portugal, from 1626 to 1820 – A search for

1172 evidence of solar forcing.

1173

1174 Moreno, J., Fatela, F., Leorri, E., Araújo, M.F., Moreno, F., De la Rosa, J.M., Freitas, M.C.,

1175 Valente, T. and Corbett, R., 2015. Bromine enrichment in marsh sediments as a marker of

1176 environmental changes driven by Grand Solar Minima and Anthropogenic activity (Caminha,

1177 NW of Portugal). *Science of the Total Environment* 506–507, 554–566.



1178

1179 Moreno, J., Fatela, F., Leorri, E., De la Rosa, J., Pereira, I., Araújo, M.F., Freitas, M.C.,  
1180 Corbett, R. and Medeiros, A., 2014. Marsh benthic foraminifera response to estuarine  
1181 hydrological balance driven by climate variability over the last 2000 years (Minho estuary,  
1182 NW Portugal). *Quaternary Research* 82, 318–330.

1183

1184 Moreno, J., Fatela, F., Andrade, C., Cascalho, J., Moreno, F. and Drago, T., 2005. Living  
1185 foraminiferal assemblages from the Minho and Coura estuaries (Northern Portugal): a  
1186 stressful environment. *Thalassas* 21, 17–28.

1187

1188 Morrissey, E.M., Gillespie, J.L., Morina, J.C. and Franklin, R.B., 2014. Salinity affects  
1189 microbial activity and soil organic matter content in tidal wetlands. *Global Change Biology*  
1190 20, 1351–1362.

1191

1192 Neubauer, S.C., Franklin, R.B. and Berrier, D.J., 2013. Saltwater intrusion into tidal  
1193 freshwater marshes alters the biogeochemical processing of organic carbon *Biogeosciences*  
1194 Discussions 10, 10685–10720.

1195

1196 Neukom, R. Gergis, J. 3, Karoly, D.J., Wanner, H., Curran, M., Elbert, J., González-Rouco,  
1197 F., Linsley, B.K, Moy, A.D., Mundo, I.,10, Raible, C.C.,1,11, Steig, E.J., van Ommen, T.,  
1198 Vance, T. Villalba, R., Zinke, J. and Frank, D., 2014. Inter-hemispheric temperature  
1199 variability over the past millennium. *Nature Climate Change* 4, 362–367.

1200

1201 Neuparth, T., Correia, A.D., Costa, F.O., Lima, G. and Costa, M.H., 2005. Multi-level  
1202 assessment of chronic toxicity of estuarine sediments with the amphipod *Gammarus*  
1203 *locusta*: I. Biochemical endpoints. *Marine Environmental Research* 60, 69–91.

1204

1205 Nittrouer, C.A., Sternberg, R.W., Carpenter, R. and Bennett, J.T., 1979. The use of <sup>210</sup>Pb  
1206 geochronology as a sedimentological tool: application to the Washington Continental Shelf.  
1207 Marine Geology 31, 297–316.

1208

1209 Obrist, D., Tas, E., Peleg, M., Matveev, V., Fain, X., Asaf, D. and Luria, M., 2011. Bromine-  
1210 induced oxidation of mercury in the mid-latitude atmosphere. Nature Geoscience 4, 22–26.

1211

1212 Panno, S.V., Hackley, K.C., Hwang, H.H., Greenberg, S.E., Krapac, I.G., Landsberger, S.  
1213 and O’Kelly, D.J., 2006. Characterization and identification of Na-Cl sources in ground  
1214 water. Ground Water 44, 176–187.

1215

1216 Parnell, A., Haslett, J., Allen, J., Buck, C. and Huntley, B., 2008. A flexible approach to  
1217 assessing synchronicity of past events using Bayesian reconstructions of sedimentation  
1218 history. Quaternary Science Reviews 27, 1872–1885.

1219

1220 Paula, J., Silva, I.C., Francisco, S.M. and Flores, A.V., 2006. The use of artificial benthic  
1221 collectors for assessment of spatial patterns of settlement of megalopae of *Carcinus*  
1222 *maenas* (L.) (Brachyura: Portunidae) in the lower Mira Estuary, Portugal. Hydrobiologia 557,  
1223 69–77.

1224

1225 Persicke, U., Gerlach, A. and Heiber, W., 1999. Zur botanischen Zusammensetzung von  
1226 Treibsel der niedersächsischen Deichvorländer und Deichabsnitte. Drosera 1, 23–34.

1227

1228 Poffenbarger, H.J., Needelman, B.A. and Megonigal, J.P., 2011. Salinity influence on  
1229 methane emissions from tidal marshes. Wetlands 31, 831–842.

1230

1231 Raimund, S., Quack, B., Bozec, Y., Vernet, M., Rossi, V., Garçon, V., Morel, Y. and Morin  
1232 P., 2011. Sources of short-lived bromocarbons in the Iberian upwelling system.  
1233 Biogeosciences 8, 1551–1564.

1234

1235 Reis, P.A., Guilhermino, L., Antunes, C., and Sousa, R., 2014. Assessment of the ecological  
1236 quality of the Minho estuary (Northwest Iberian Peninsula) based on metal concentrations in  
1237 sediments and in *Corbicula fluminea*. Limnetica 33, 161–174.

1238

1239 Rhew, R.C., Whelan, M.E. and Min, D.-H., 2014. Large methyl halide emissions from south  
1240 Texas saltmarshes. Biogeosciences 11, 6427–6434.

1241

1242 Rhew, R.C. and Mazéas, O., 2010. Gross production exceeds gross consumption of methyl  
1243 halides in northern California salt marshes. Geophysical Research Letters 37, L18813, 5 p.

1244

1245 Rhew, R.C., Miller, B.R., Bill, M., Goldstein, A.H. and Weiss, R.F., 2002. Environmental and  
1246 biological controls on methyl halide emissions from southern California coastal salt  
1247 marshes. Biogeochemistry 60, 141–161.

1248

1249 Rhew, R.C., Miller, B.R. and Weiss, R.F., 2000. Natural methyl bromide and methyl chloride  
1250 emissions from coastal salt marshes. Nature 403, 292–295.

1251

1252 Roberts, T.J., Martin, R.S. and Jourdain, L., 2014. Reactive bromine chemistry in Mount  
1253 Etna's volcanic plume: the influence of total Br, high-temperature processing, aerosol  
1254 loading and plume–air mixing. Atmospheric Chemistry and Physics 14, 11201–11219.

1255

1256 Saito, T. and Yokouchi, Y., 2006. Diurnal variation in methyl halide emission rates from  
1257 tropical ferns. *Atmospheric Environment* 40, 2806–2811.

1258

1259 Shaw, S.D., Blum, A., Weber, R., Kannan, K., Rich, D., Lucas, D., Koshland, C.P., Dobraca,  
1260 D., Hanson, S. and Birnbaum, L.S., 2010. Halogenated flame retardants: do the fire safety  
1261 benefits justify the risks? *Reviews on Environmental Health* 25, 261–305.

1262

1263 Smith, J.N., 2001. Why should we believe  $^{210}\text{Pb}$  sediment geochronologies? *Journal of*  
1264 *Environmental Radioactivity* 55, 121–123.

1265

1266 Soon, W., Velasco Herrera, V.M., Selvaraj, K., Traversi, R., Usoskin, I., Chen, C.-T.A., Lou,  
1267 J.-Y., Kao, S.-J., Carter, R.M., Pipin, V., Severi, M. and Becagli, S., 2014. A review of  
1268 Holocene solar-linked climatic variation on centennial to millennial timescales: physical  
1269 processes, interpretative frameworks and a new multiple cross-wavelet transform algorithm.  
1270 *Earth Science Reviews* 134, 1–15.

1271

1272 Spohn, M., Babka, B. and Giani, L., 2013. Changes in soil organic matter quality during sea-  
1273 influenced marsh soil development at the North Sea coast. *Catena* 107, 110–117.

1274

1275 Spohn, M. and Giani, L., 2012. Carbohydrates, carbon and nitrogen in soils of a marine and  
1276 a brackish marsh as influenced by inundation frequency. *Estuarine, Coastal and Shelf*  
1277 *Science* 107, 89–96.

1278

1279 Steinhilber, F., Abreu, J.A., Beer, J., Brunner, I., Christl, M., Fischer, H., Heikkilä, U., Kubik,  
1280 P.W., Mann, M., McCracken, K.G., Miller, H., Miyahara, H., Oerter, H. and Wilhelms, F.,

1281 2012. 9,400 years of cosmic radiation and solar activity from ice cores and tree rings.  
1282 Proceedings of the National Academy of Sciences 109, 5967–5971.  
1283

1284 Usoskin, I.G. and Kovaltsov, G.A., 2008. Cosmic rays and climate of Earth: Possible  
1285 connection, *Comptes Rendus Geoscience* 340, 441–450.  
1286

1287 Vale, L.M. and Dias, J.M., 2011. The effect of tidal regime and river flow on the  
1288 hydrodynamics and salinity structure of the Lima Estuary: Use of a numerical model to  
1289 assist on estuary classification, SI 64 (Proceedings of the 11th International Coastal  
1290 Symposium), Szczecin, Poland, pp. 1604–1608.  
1291

1292 Taborda, R., Dias, J.M.A., 1991. Análise da sobre-elevação do nível do mar de origem  
1293 meteorológica durante os temporais de 1978 e 1981. *Geonovas*, SI 1, 89–97.  
1294

1295 Thiéblemont, R., Matthes, K., Omrani, N.-E., Kodera, K. and Hansen, F., 2015. Solar forcing  
1296 synchronizes decadal North Atlantic climate variability. *Nature Communications* 6:8268. 8 p.  
1297

1298 Trigo, R.M., Vaquero, J.M., Alcoforado, M.J., Barriendos, M., Taborda, J., García-Herrera R.  
1299 and Luterbacher, J., 2009. Iberia in 1816, the year without a summer. *International Journal*  
1300 *of Climatology* 29, 99–115.  
1301

1302 Van de Broek, M., Temmerman, S., Merckx, R. and Govers, G., 2016. The importance of an  
1303 estuarine salinity gradient on soil organic carbon stocks of tidal marshes. *Biogeosciences*  
1304 *Discussions*, doi:10.5194/bg-2016-285.  
1305

1306 Varner, R.K., Crill, P.M. and Talbot, R.W., 1999. Wetlands: A potentially significant source  
1307 of atmospheric methyl bromide and methyl chloride, *Geophysical Research Letters* 26,  
1308 2433– 2435.

1309

1310 Vinogradov, A.P., 1959. *The Geochemistry of Rare and Dispersed Elements in Soils*.  
1311 Second edition, Consultants Bureau, New York, 209 p.

1312

1313 Weinberg, I., Bahlmann, E., Eckhardt, T., Michaelis, W. and Seifert, R., 2015. A halocarbon  
1314 survey from a seagrass dominated subtropical lagoon, Ria Formosa (Portugal): flux pattern  
1315 and isotopic composition. *Biogeosciences* 12, 1697–1711.

1316

1317 Weinberg, I., Bahlmann, E., Michaelis, W. and Seifert, R., 2013. Determination of fluxes and  
1318 isotopic composition of halocarbons from seagrass meadows using a dynamic flux  
1319 chamber. *Atmospheric Environment* 73, 34–40.

1320

1321 Wishkerman, A., Gebhardt, S., McRoberts, C.W., Hamilton, J.T.G., Williams, J. and  
1322 Keppler, F., 2008. Abiotic methyl bromide formation from vegetation and its strong  
1323 dependence on temperature. *Environmental Science & Technology* 42, 6837–6842.

1324

1325 Wuosmaa, A. M. and Hager, L. P., 1990. Methyl chloride transferase: a carbocation route  
1326 for biosynthesis of halometabolites, *Science* 249, 160–162.

1327

1328 Yvon-Lewis, S.A., Saltzman, E.S. and Montzka, S.A., 2009. Recent trends in atmospheric  
1329 methyl bromide: analysis of post-Montreal Protocol variability. *Atmospheric Chemistry and*  
1330 *Physics* 9, 5963–5974.

1331

1332 Ziegler, M., Jilbert, T., de Lange, G.J., Lourens L.J. and Reichart, G.-J., 2008. Bromine  
1333 counts from XRF scanning as an estimate of the marine organic carbon content of sediment  
1334 cores. *Geochemistry Geophysics Geosystems* 9, Q05009, 6 p.

1335

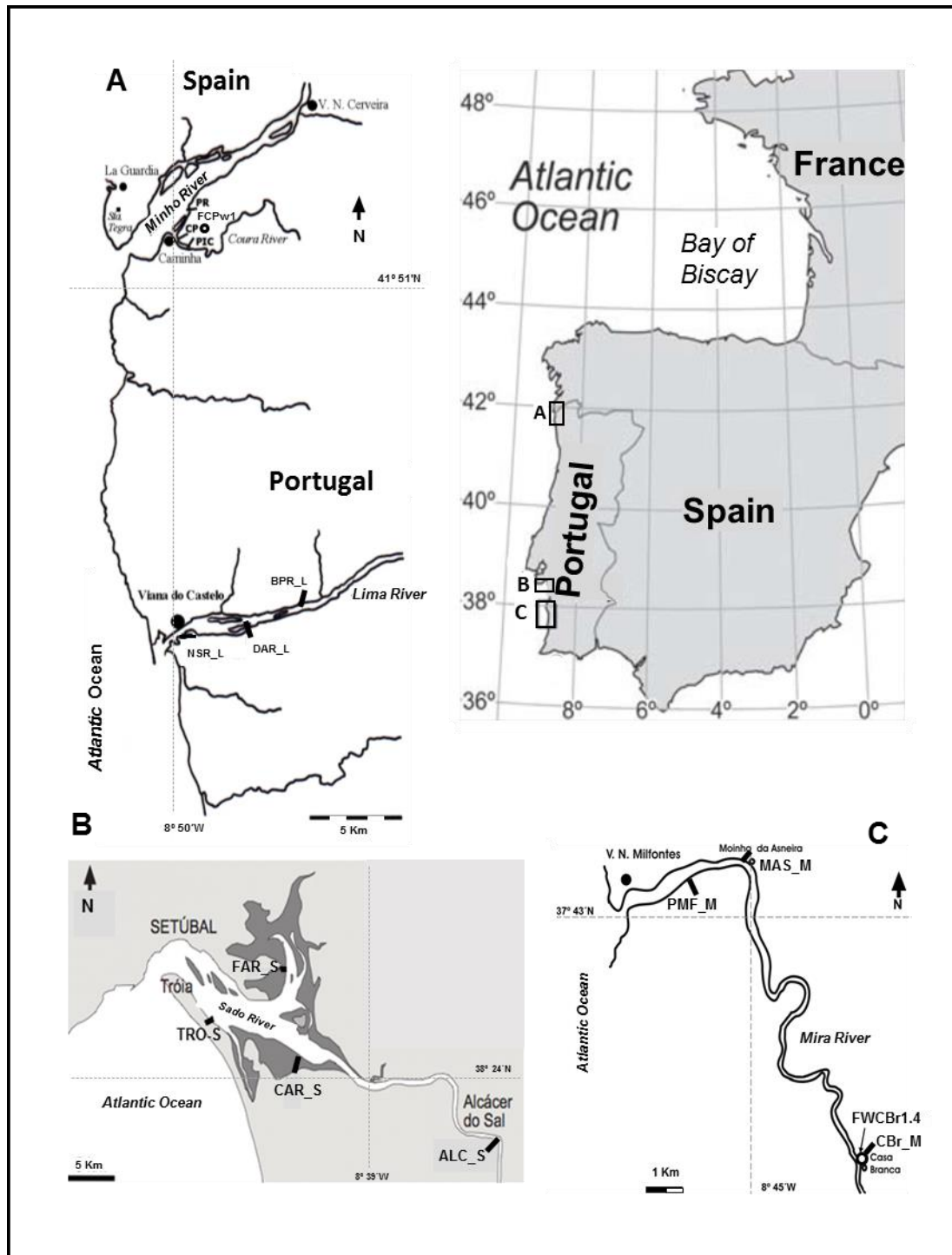
1336 <http://www.icnf.pt/portal/ap/r-nat/rnet/geo>

1337 <http://www.noaa.gov/>

1338

1339

1340



1341  
1342

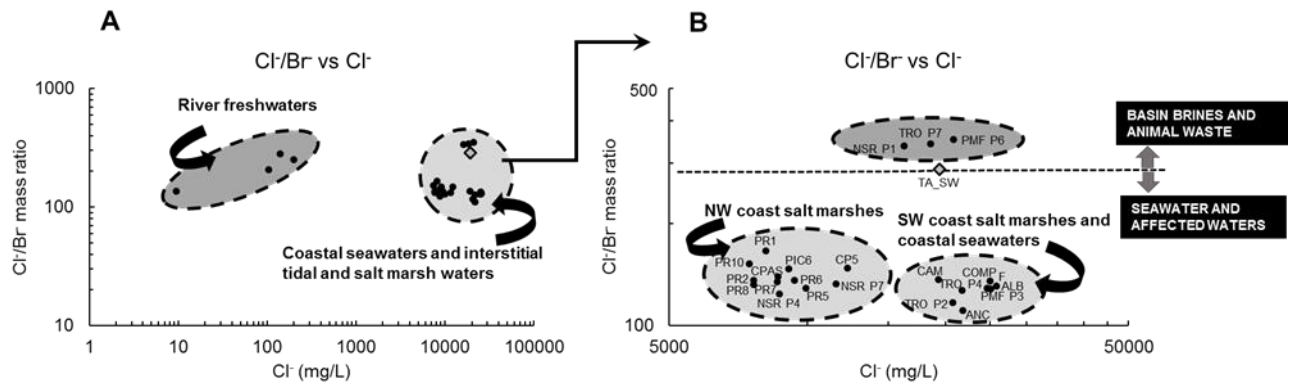
1343 **Figure 1.** A. Study areas general location; B. Minho and Lima estuaries (NW coast); C. Sado estuary (SW  
 1344 coast); D. Mira estuary (SW coast). The location of the complete sampling set is also signalled. This includes  
 1345 thirteen surface sampling transects across the four tidal salt marshes (where both interstitial waters and  
 1346 sediments have been collected), and the two sediment cores obtained in the high marsh zones of the  
 1347 Caminha (FCPw1; Minho estuary; 1.55 m above mean sea level; 41°52'37.0" N and 8°49'28.0" W) and Casa  
 1348 Branca (FWCBr1.4; Mira estuary; 1.74 m above mean sea level; 37°40'03.7" N and 8°43'12.7" W) salt  
 1349 marshes.  
 1350

1351

1352



1353



1354

1355 **Figure 2.** Cl<sup>-</sup>/Br<sup>-</sup> mass ratios vs. Cl<sup>-</sup> concentrations of (surface and interstitial) water samples and potential  
1356 sources (zones and theoretical limits from Panno et al., 2006). **A.** Clusters of freshwater (riverine), marine, and  
1357 impacted water samples are indicated (i.e., tidal and salt marsh interstitial waters). **B.** Clusters of interstitial  
1358 waters from NW and SW coastal salt marshes. Marine water samples are in the same group as the SW coast  
1359 salt marshes interstitial water. A group of three anomalous samples (TRO\_P7, NSR\_P1 and PMF\_P6) is also  
1360 identified. The diamond represents a typical marine sample.

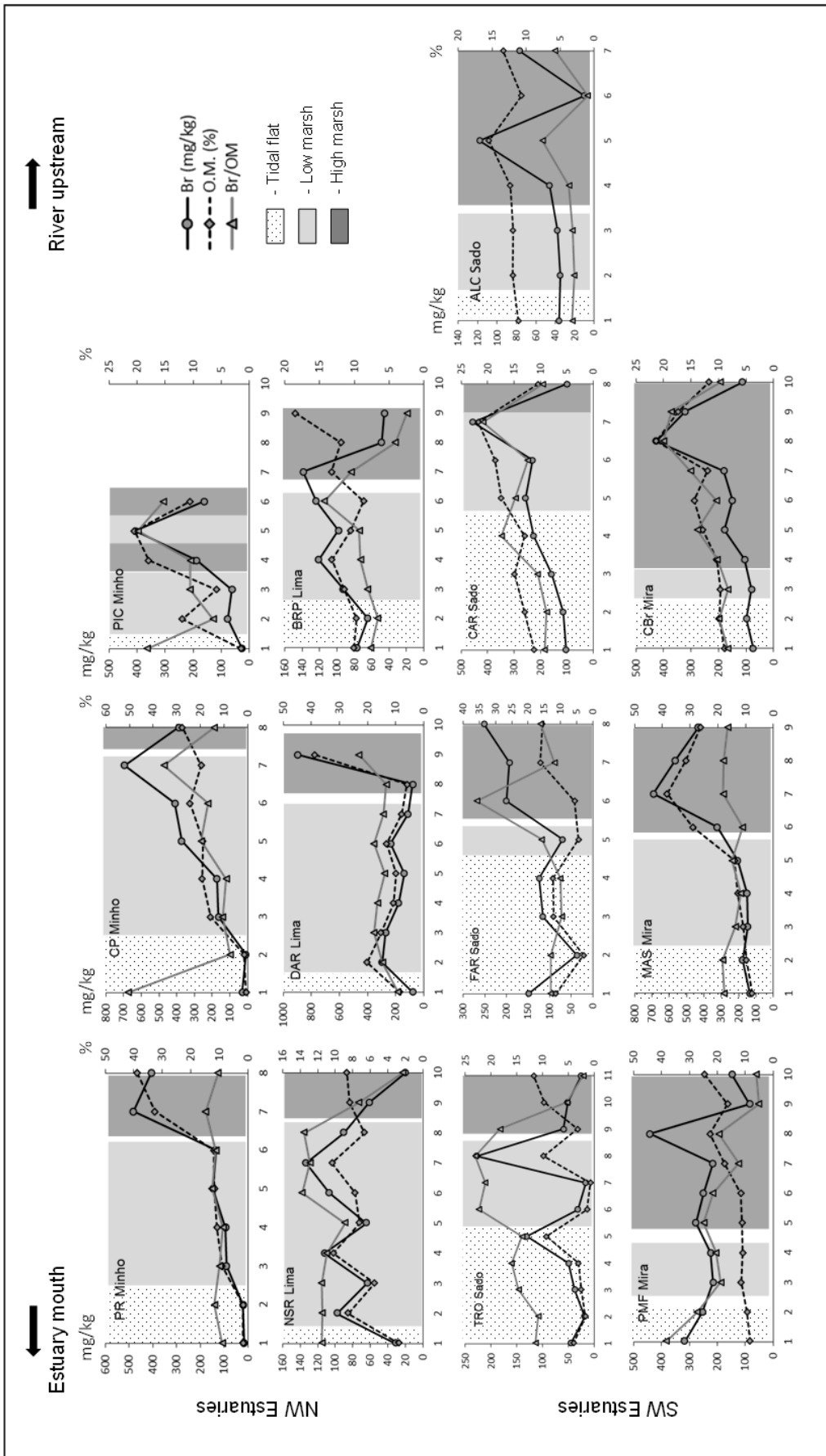


Figure 3. Bromine and organic matter contents (OM) of superficial tidal salt marsh sediment transects from Minho, Lima, Sado and Mira estuaries.

1362  
1363

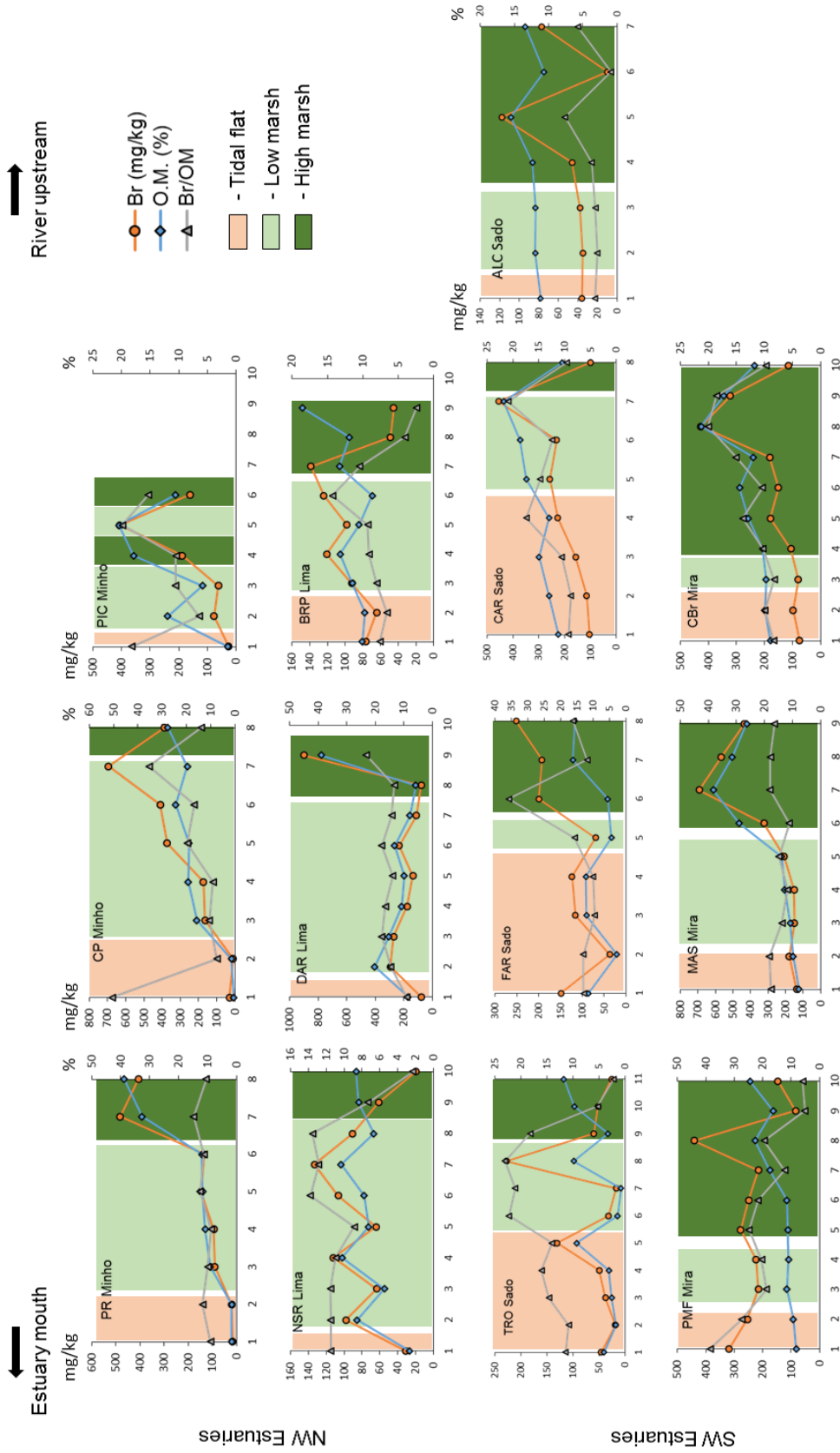
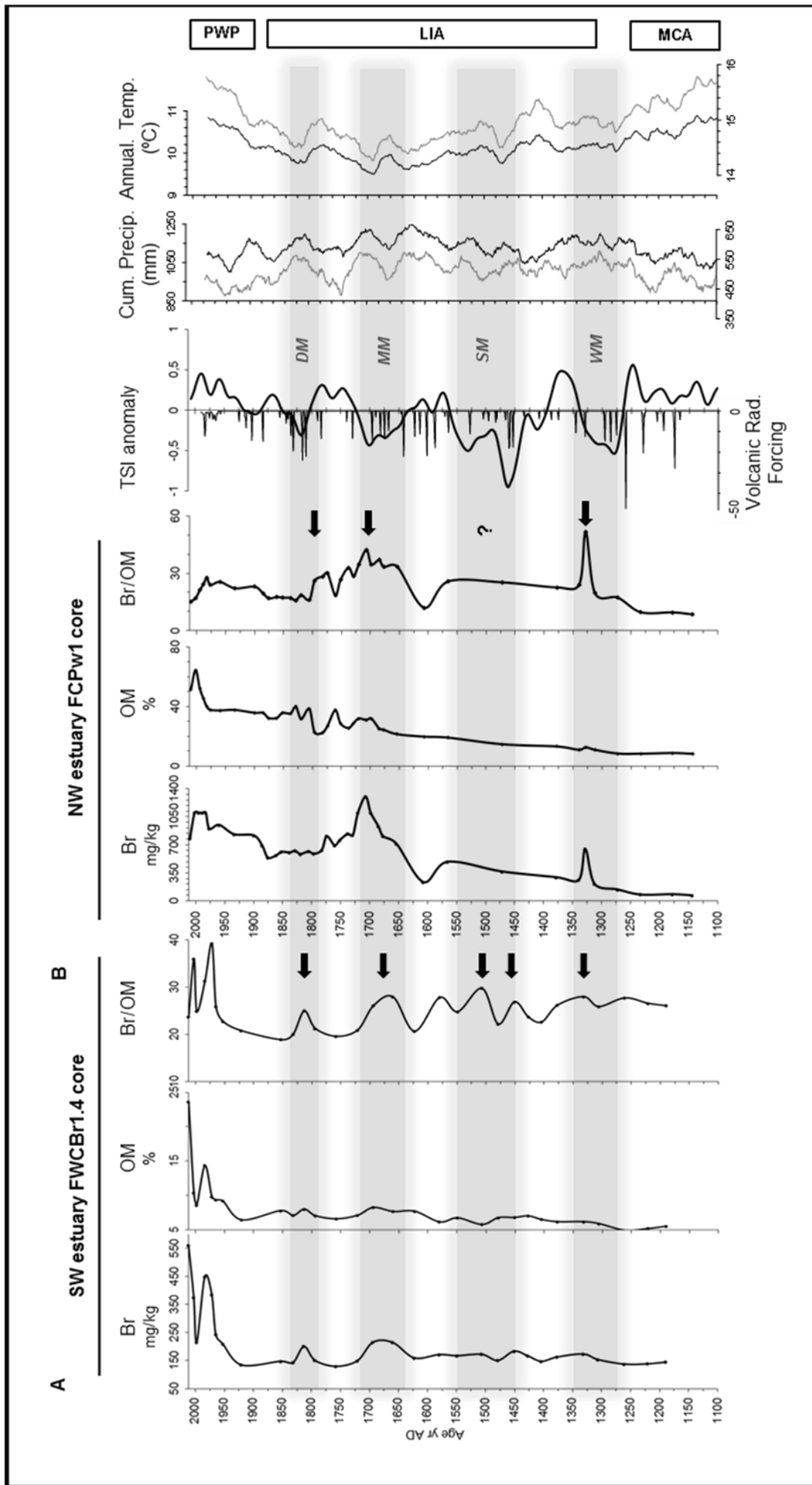
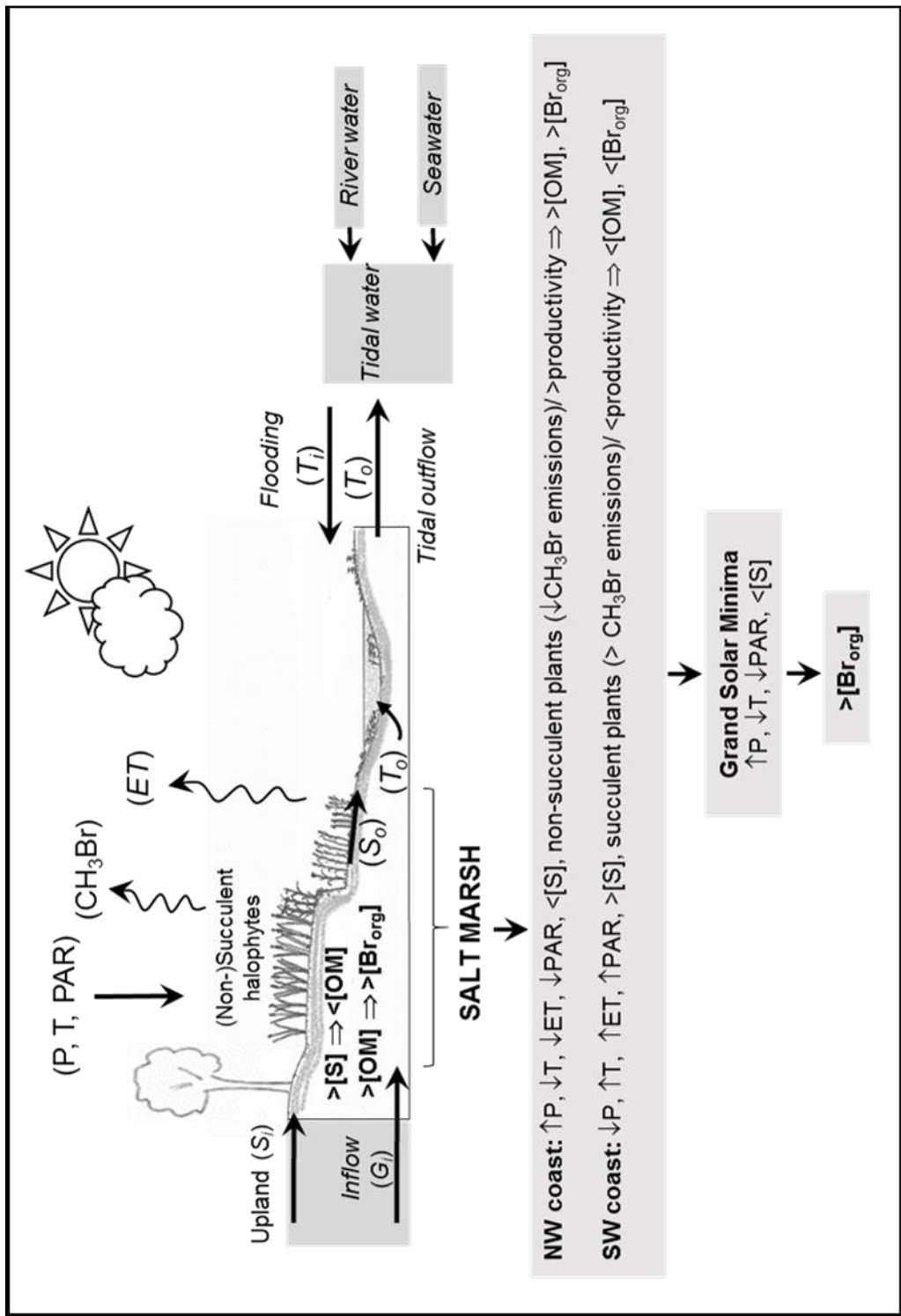


Fig 3. Bromine and organic matter (OM) contents of superficial tidal salt marsh sediment transects from Minho, Lima, Sado and Mira estuaries.



**Figure 4.** FCPw1 and FWCB1.4 cores geochemical data: Br (mg/kg), OM (%) and Br/OM ratios. Other data represented are: TSI anomaly using a 21-year running average reconstruction (Steinhilber et al., 2012); volcanic radiative forcing (black bars) after Crowley (2000); cumulative precipitation and annual temperature (31-year running averages) for NW coast (black lines and top axis) and SW coast (grey lines and bottom axis) of Portugal (Gómez-Navarro et al., 2011). DM – Dalton Minimum; MM – Maunder Minimum; SM – Spörer Minimum; WM – Wolf Minimum.

1365  
 1366  
 1367  
 1368  
 1369  
 1370  
 1371  
 1372  
 1373  
 1374



**Figure 5.** Conceptual model for the Br cycling in the W Portuguese coast salt marshes, including the most important elements influencing the Br pool in soils/sediments. (P– Precipitation; T– Temperature; PAR– Photosynthetically Active Radiation; ET– Evapotranspiration; S– Surface water inflow; S<sub>o</sub>– Surface water outflow; G<sub>i</sub>– Ground water inflow; T<sub>i</sub>– Tidal water outflow; T<sub>o</sub>– Tidal water outflow; [S]– Salinity; [OM]– Soil/Sediment Organic Matter content; [Br<sub>org</sub>]– Soil/Sediment Organic Bromine content).

**Table 1.** Bromide concentrations in surface water (river freshwater, estuarine and coastal seawater) samples and in marsh interstitial water samples (Minho, Lima, Sado and Mira tidal salt marshes).

Surface and interstitial waters	NW coast				SW coast			
	Minho		Lima		Sado		Mira	
Zone	Br <sup>-</sup> (mg/L)	Salinity (‰)	Br <sup>-</sup> (mg/L)	Salinity (‰)	Br <sup>-</sup> (mg/L)	Salinity (‰)	Br <sup>-</sup> (mg/L)	Salinity (‰)
River	<d.l.	0.0	0.07	0.0	0.8	0.3	0.5	0.2
Estuary mouth	141	32.5	—	—	—	—	—	—
Coastal seawater	197	35.2	197	35.2	185	35.7	197	35.4
Tidal flat	52 (48-55)*	9.5 (2-17)*	48	24.6	177	31.8	—	—
Low marsh	71 (64-83)*	14.5 (10-18)*	70	14.4	171	31.4	195	37.0
High marsh	56 (49-62)*	12.6 (11-15)*	87	13.5	54	26.6	59	30.6
Marsh transect references	PR; CP; PIC		NSR-L		TRO-S		PMF-M	
Distance to river mouth (km)	3.8 - 4.8		2.0		14.0		2.0	

\*Average from three transects and range

d.l. detection limit (0.01 mg/L Br<sup>-</sup>)

1375

1376

1377

1378

1379

1380

1381

**Table 2.** Bromine content and OM contents in the surface sediment cross shore transects from the Minho, Lima, Sado and Mira intertidal domains (tidal flat, low marsh and high marsh).

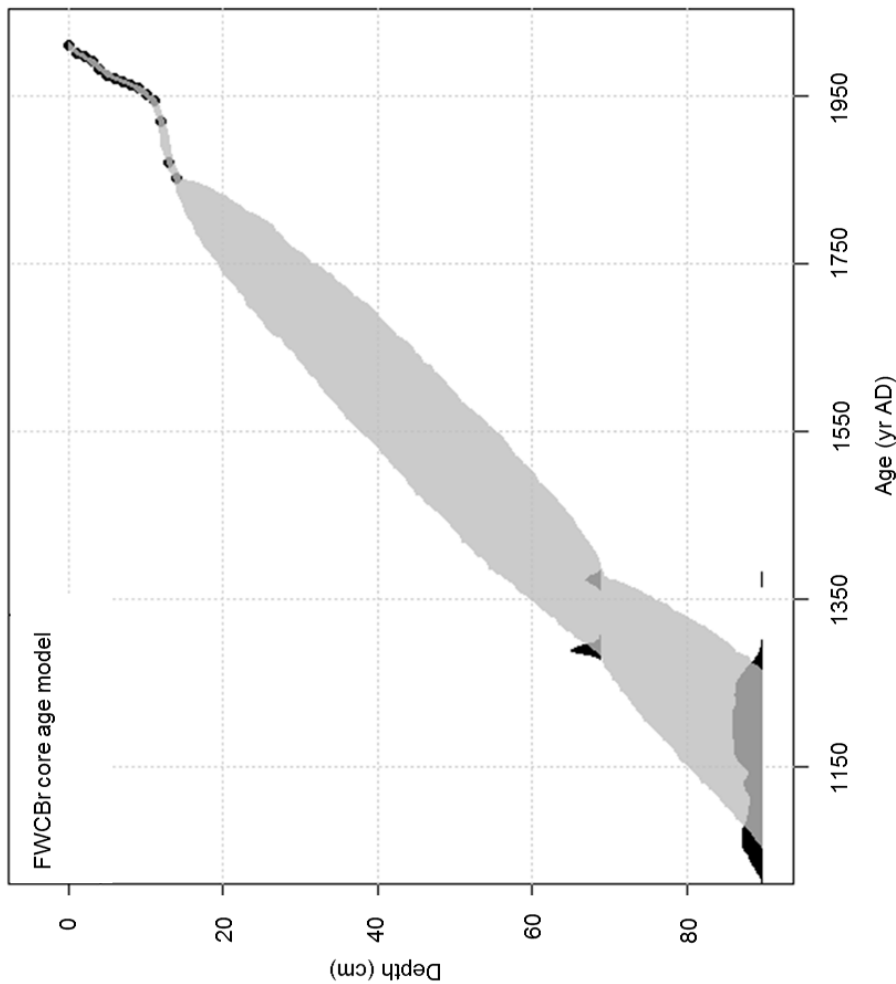
Surface sediment samples / Estuaries	NW coast				SW coast			
	Minho		Lima		Sado		Mira	
Zone	Br (mg/kg)	OM (%)	Br (mg/kg)	OM (%)	Br (mg/kg)	OM (%)	Br (mg/kg)	OM (%)
Tidal Flat	21 (11-30)*	1.4 (0.6-1.7)*	71 (31-79)*	8.6 (2.7-10.1)*	83 (19-226)**	11.5 (1.7-15.0)**	158 (75-318)*	8.8 (7.7-9.9)*
Low Marsh	133 (62-695)*	15.0 (5.9-24.4)*	110 (64-296)*	11.0 (5.5-20.2)*	53 (17-456)**	8.2 (0.8-21.8)**	152 (80-224)*	11.2 (9.7-12.8)*
High Marsh	389 (162-482)*	27.7 (10.6-38.8)*	49 (45-900)*	13.3 (5.9-38.9)*	81 (10-252)**	11.7 (3.3-16.3)**	233 (85-693)*	16.9 (11.2-38.3)*
Marsh transect/cores surface references	PR; CP; PIC		NSR_L; DAR_L; BPR_L		TRO_S; CAR_S; FAR_S; ALC_S		PMF_M; MAS_M; CBr_M	
Distance to river mouth (km)	3.8 - 4.8		2; 5; 8.5		14; 19; 24; 43.5		2; 3.5; 13	
Correlation coefficient Br vs.OM (p < 0.001)	0.86 (N= 21)		0.89 (N= 28)		0.67 (N= 34)		0.79 (N= 29)	

\*Average (median) from three transects and range

\*\*Average (median) from four transects and range

1382

1383



Core/Sample	Depth (cm)	$\delta^{13}\text{C}$ ‰	Conventional radiocarbon age	$\Delta^{14}\text{C}$ ‰	Calibrated years AD (2 Sigma range)
FW CBr 2.0 CM 70	69-70	-25.0	720 +/- 30 BP	-85.7±3.4	1260 to 1295
FW CBr 2.0 CM 91	90-91	-25.6	920 +/- 30 BP	-108.2±3.3	1025 to 1190

Depth (cm)	$^{137}\text{Cs}$	2-sigma	$^{210}\text{Pb}$	2-sigma	$^{214}\text{Pb}$	2-sigma	$^{210}\text{Pb}$ excess
0.5	5.56	2.27	152.5	30.6	37.5	6.76	115
1.5	5.44	1.6	84.52	20.11	40.02	3.78	44.5
2.5	6.95	1.63	72.48	20.36	38.38	3.9	34.1
3.5	8.78	2.13	98.24	21.85	37.22	5.58	61.02
4.5	10.64	2.18	70.55	21.47	34.65	5.25	35.9
5.5	13.23	2.23	53.13	21.05	32.45	4.79	20.68
6.5	19.19	2.32	48.51	25.88	34.29	3.97	14.22
7.5	23.69	2.73	46.97	17.43	36.53	6.44	10.44
8.5	14.41	2.04	54.26	18.92	42.94	5.77	11.32
9.5	6.74	1.81	58.57	20.37	41.42	4.24	17.15
10.5	6.4	1.72	52.57	18.23	40.33	4.8	12.24
11.5	5.45	1.65	65.43	19.23	41.41	3.99	24.02
12.5	2.92		65.13	22.17	47.18	4.21	17.95
13.5	2.37		53.57	21.12	51.31	5.19	2.26
14.5	2.58		56.08	21.57	52.17	5.83	3.91
15.5	2.5		41.48	19.35	43.05	4.29	-1.57

Pb and Cs isotopes contents (Bq kg<sup>-1</sup>)

Appendix A. Age model for the core FWCBr and estimated 2  $\sigma$  errors, based on two AMS  $^{14}\text{C}$  dates, performed on total organic sediment, and  $^{210}\text{Pb}$  and  $^{137}\text{Cs}$  chronology. The data interpolation was obtained with Bchron 4.1 software.

1385 **Appendix B.** Geochemical data from the sediment core FWCB (Casa Branca salt marsh;  
1386 Mira estuary).

Depth (cm)	Br (ppm)	OM (%)	Br/OM	Age (AD years)
0-1	560	23.6	23.7	2012
1-2	374	10.4	36.0	2003
2-3	214	8.6	24.9	1998
4-5	448	14.3	31.2	1984
6-7	385	9.8	39.3	1972
8-9	242	9.4	25.8	1965
10-11	209	9.2	22.7	1953
12-13	134	6.5	20.7	1921
14-15	147	7.8	18.8	1853
16-17	142	7.1	20.0	1832
18-19	200	8.0	24.9	1813
20-21	150	7.1	21.2	1794
24-25	129	6.6	19.5	1758
28-29	149	7.1	20.9	1721
31-32	215	8.3	26.0	1694
35-36	214	7.7	27.9	1660
39-40	159	7.7	20.6	1623
43-44	171	6.2	27.8	1580
47-48	167	6.7	24.8	1549
52-53	172	5.8	29.7	1507
55-56	150	6.8	22.1	1479
58-59	183	6.8	26.9	1451
61-62	166	7.0	23.6	1427
64-65	147	6.5	22.6	1404
68-69	162	6.2	26.2	1377
72-73	173	6.2	28.0	1332
75-76	153	5.9	25.9	1306
80-81	137	4.9	27.7	1261
85-86	138	5.2	26.5	1221
89-90	144	5.5	26.0	1190

1387

1388

1389

1390

1391